



**Politecnico
di Torino**

POLITECNICO DI TORINO
Department of Mechanical and Aerospace Engineering
Master of Science in Automotive Engineering
Academic Year 2021/2022
December 2022

**Electromagnetic Dampers for Motorcycle Suspensions:
Control Strategies and Performance Assessment**

Supervisor: **Prof. Andrea Tonoli**

Candidate:

Ishan Sharma

Acknowledgment

This thesis project has been developed in the *Department of Mechanical and Aerospace Engineering* (Polytechnic of Turin).

I am very grateful to Prof. Tonoli, for providing me an opportunity to work on this interesting project regarding regenerative dampers.

I am very thankful Marco Puliti who was helpful in every way possible during the initial part of this project. He helped in developing the starting model in Matlab and Simulink for this project, with our weekly online meetings. Next, I would like to express my gratitude to Gennaro Sorrentino and Manfredi Tornabene, who joined later on this project. They were very kind and patient with me and were very helpful with their valuable insights and feedback during the last months. I got to learn a lot from all of them.

I would further like to extend my deepest and sincerest gratitude to my friends who helped me during the course, whether in studies or in personal situations: Michele Settembrino, Danilo Lunetta, Jurgen Ascurra, Filippo Bertoli and others. I would like to thank especially Lorenzo Giorgis for his constant support in all situations.

Finally, I cannot thank enough my parents for their constant support in my pursuing this field. And I would like to offer my humble obeisances and earnest gratitude to the Supreme Personality of Godhead for everything.

Abstract

With increasing awareness of reducing emissions and conservation of energy, along with increasing comfort and road safety, more and more companies are studying and developing regenerative suspensions, both in the motorcycle and automotive field. These systems can not only recover some part of the energy otherwise dissipated by the suspension in the form of heat, but also can help reduce CO₂ emissions.

This led to the advent of active and semi-active suspension systems, which are the most advanced suspension systems technology at present. The semi-active suspensions are more widely used in the motorcycles since more than a decade, because they are able to provide the best compromise between cost and performance (with low power request). Thanks to the hybridization and electrification of the vehicles in general, active suspensions would be the next step, as they are already implemented in the automotive industry. Active devices provide all the forces between the vehicle body and the unsprung mass, and work in all four quadrants of the force-velocity plot, thus require higher power than semi-active systems. However, the performance is much better than the semi-active ones.

To this end, this thesis project focuses on the study and implementation of possible active control strategies for motorcycle applications. For this purpose, an electrohydrostatic regenerative shock absorber is used which is able to convert hydraulic power into electric power, and vice-versa. To study the damper behaviour in dynamic conditions, a mono-corner (quarter car) model was used which represents the front suspension of a motorcycle. First, an ideal damper model was created in Matlab and Simulink. Then to simulate a real passive damper, a lookup table was used which comes from experimental characterization. Furthermore, skyhook and groundhook control strategies were implemented to the model and the efficiency map of the motor was also used to account for losses during power evaluation. After trying different combinations of the damping coefficients, finally their simulation results are compared with each other to ascertain the optimal configuration.

Contents

1. Introduction	1
1.1 Suspensions	1
1.2 Front Suspension Types	2
1.3 Rear Suspension Types	12
1.4 Controlled Suspension	17
1.4.1 Semi-active Suspensions	18
1.4.2 Active Suspensions	19
1.4.3 Regenerative Shock Absorbers	20
1.5 Thesis Motivation	22
1.6 Thesis Outline	23
2. Methodology	24
2.1 Quarter Car Model	24
2.1.1 Passive damper	25
2.1.2 Real passive damper	31
2.2 Control Strategies	34
2.2.1 Skyhook control	34
2.2.2 Groundhook control	41
3. Simulations and Results analysis	44
3.1 Ideal quarter car model	44
3.2 Quarter car with lookup table	53
3.3 Quarter car with active skyhook	61
3.4 Quarter car with active groundhook	64
4. Conclusions	69
List of figures	71
List of tables	74
Bibliography	75

1. Introduction

1.1 Suspensions

The main purposes of suspensions are to contribute to the road-holding/handling of the vehicle, to provide comfort to the rider and to keep them well isolated from the road noise. Moreover, the suspensions affect the vehicle's trim during turning, braking, accelerating and so on. Many parameters play an important role in selecting the proper front and rear suspension characteristics: the geometry of the motorcycle, the road surface, the braking performance, the conditions of use, the weight of the rider and the motorcycle, the position of the centre of gravity, the characteristics of stiffness and vertical damping of the tyres, the engine power and driving technique, among others.

Suspension Layouts

A brief overview of several suspensions layouts that have been used over the years [1]. Broadly speaking all these suspensions can be categorized in two main groups.

- The ones that use a conventional head stock for defining the steering axis, and to mount the fork.
- The ones that do not require such a frame mounted head stock.

The old style girder forks, the leading and trailing link forks and the ubiquitous telescopic forks are included in the first group. While the second group contains a myriad of designs [2].

1.2 Front Suspension Types

Head stock mounted forks

The common feature of these types of front suspension/steering systems is that they are all mounted on and steer through a steering head stock. In Fig. 1.1, it is evident how any lateral flex move the tyre contact patch away from the steering axis. This is critical because wobble can be generated or greatly increased due to this misalignment, both on an undulated surface at any speed, and on fairly smooth roads at a particular speed. Another drawback is that during braking, a large amount of leverage can be exerted on the steering head. This results in very large forces which have to be compensated by a strong and relatively heavy frame [2].

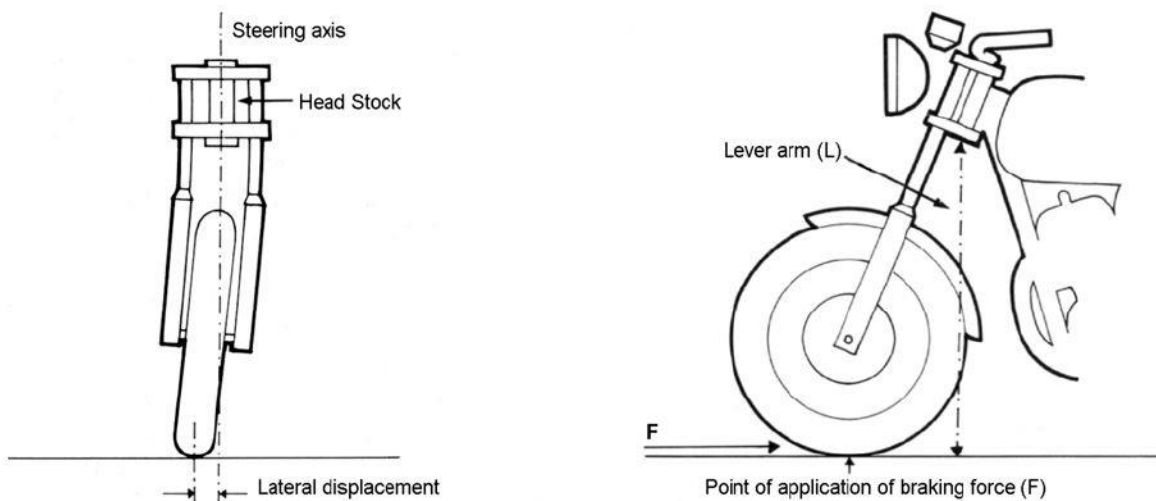


Fig. 1.1 All head stock mounted forks have these types of deflection to some degree, due to the large lever arm [2]

Telescopic forks

The telescopic fork is the most widely adopted front suspension (Fig. 1.2a). It consists of two telescopic sliders that run along the interior of the two fork tubes and form a prismatic joint between the sprung mass of the chassis and the unsprung mass of the front wheel. The telescopic fork has limited inertia around the steering head axis.

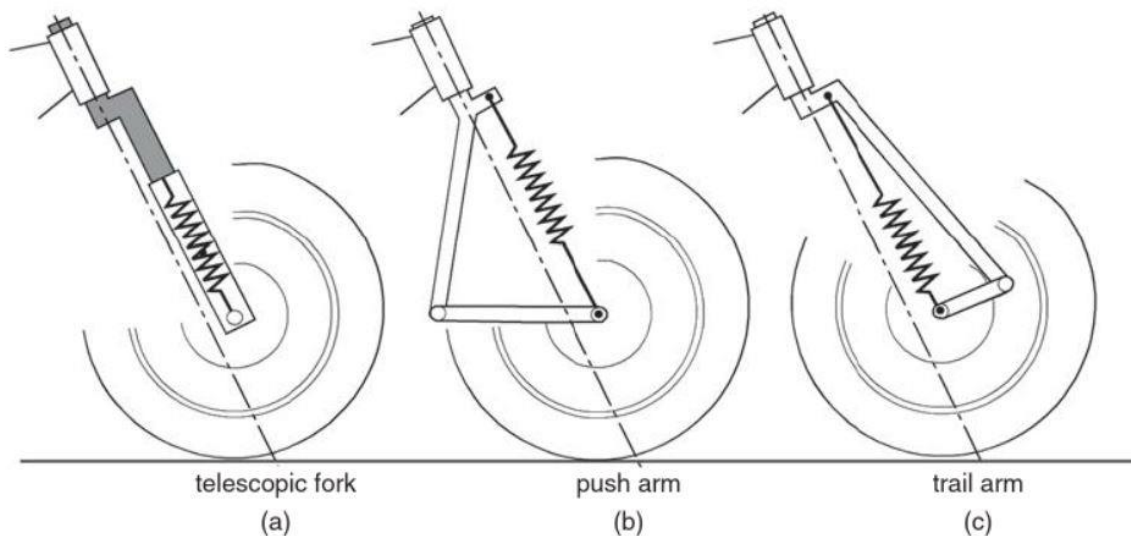


Fig. 1.2 Examples of front suspensions [1]

The main limitations of the telescopic fork are the quite high unsprung mass because it is an integral part of the wheel and the possibility of not attaining the progressive force displacement. Alternative solutions have been developed to overcome the typical drawbacks of the telescopic fork: push arm (Fig. 1.2b), trail arm (Fig. 1.2c) and four-bar linkage (like the BMW Duolever).

The design of the front arm and four-bar linkage suspensions can be done in such a way to achieve total or partial anti-dive behaviour in braking conditions [1].

Upside down (USD) forks

They are a type of telescopic forks, but they are mounted upside down. The USD forks have improved stiffness in all directions. Large wheel spindles are more commonly used, often hollow to save weight. Forks prior to USD often had a force brace or mudguard bracket above the wheel to add to the overall stiffness of the assembly, whereas the USD has only the axle to keep the two legs aligned. Thus, in this case, the size of the axle is more important. The performance of high quality USD forks is very good but they can be quite expensive [2].



Fig. 1.3 Examples of USD forks [2]

Leading link

Leading link suspension is an alternative to the telescopic fork, which has been known to be fitted to probably the best-handling motorcycles of their period – the world champion Moto Guzzis of the 1950s. The Earles fork is a variation on the same theme with longer links but has the drawback of notably higher steered inertia, used on some early MV Augusta racers and by BMW for many years.

They consist of a tubular or pressed-steel structure which connects the steering column to the link pivots and include anchorages for the suspension struts. The links are formed by a single U-shape loop around the back of the wheel or they may be independent. If the links are separate, then their ability to resist the independent movement depends on the rigidity of their attachment to the wheel spindle, just like in the case of telescopic fork. This is of usually larger diameter (hollow for lightness) and secured by extra-wide clamps, in the better design versions. However, the most weight-efficient solution would be a loop behind the wheel and a smaller diameter spindle, because the larger the diameter of the spindle, the larger will be the wheel bearings. In some cases, a well thought detailed design can have some advantages over telescopic forks. Better rigidity can be reached, with benefits in precise control and stability. Any degree of anti-dive under heavy braking can be easily designed and the lack of stiction enhances the sensitivity to small undulations considerably. The precise wheel travel path is dependent on the relative heights of the wheel spindle and the link pivots (see Fig. 1.4). These forks are generally not suitable for the large movement on the modern off-road motorcycles, due to the curved nature of the wheel travel path. Telescopic forks are better for these applications, in general [2].

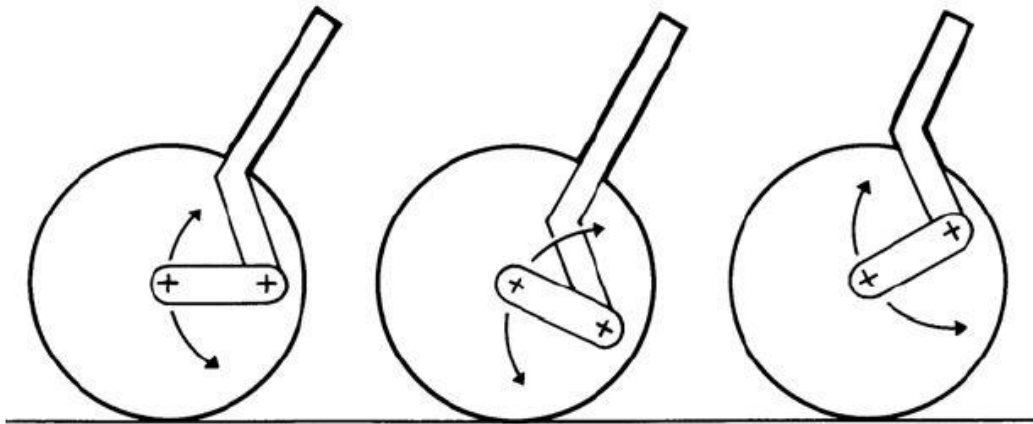


Fig. 1.4 In leading link forks, the relative heights of link pivots and wheel spindle decides the wheel travel path [2]

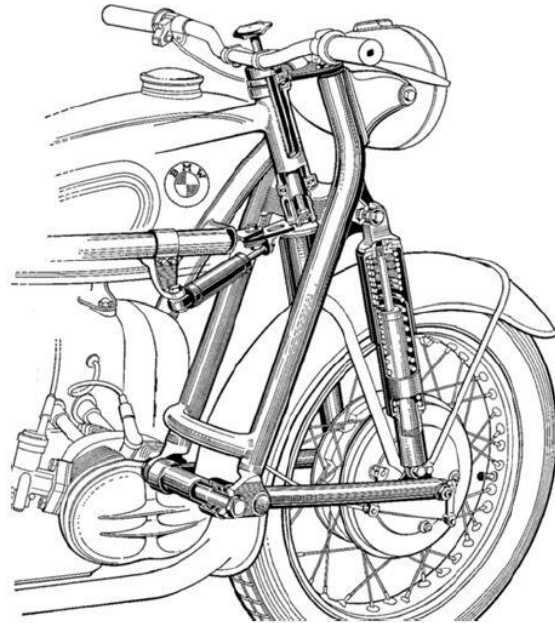


Fig. 1.5 Examples of leading link forks [2]

Trailing link

They are different from the leading link forks only slightly because the link pivots are in front of the wheel spindle, rather than behind. Since the bulk of the mass is relatively at a long distance from the steering axis, it has a drawback of increased steering inertia [2].

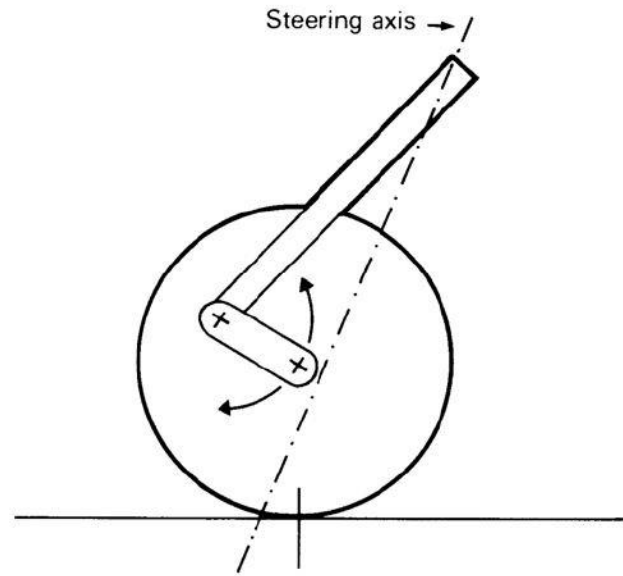


Fig. 1.6 Examples of trailing link forks [2]

Alternative to head stock mounted forks can be broadly categorized by the following four groups:

- Hub centre steered
- Double link
- McPherson strut based
- Virtual steering axis

Hub centre steered

They generally have a non-rotating but steerable hub of large diameter, which is mounted on a king-pin located within the hub. Another hub, forming part of the wheel, and of larger diameter is mounted on the first hub with the help of large diameter ball races. The steering axis is defined by the centre line of the king-pin axis, so the only flexure that can allow the tyre to deflect away from this axis, is in the hubs and the wheel themselves. It must be taken into account that any play or

wear in the king-pin bearings or bushes will permit the undesired lateral displacement.

Some suspensions that come under this category includes: Ner-a-car, Difazio (Fig. 1.7), Mead and Tomkinson, Bimota Tesi [2].

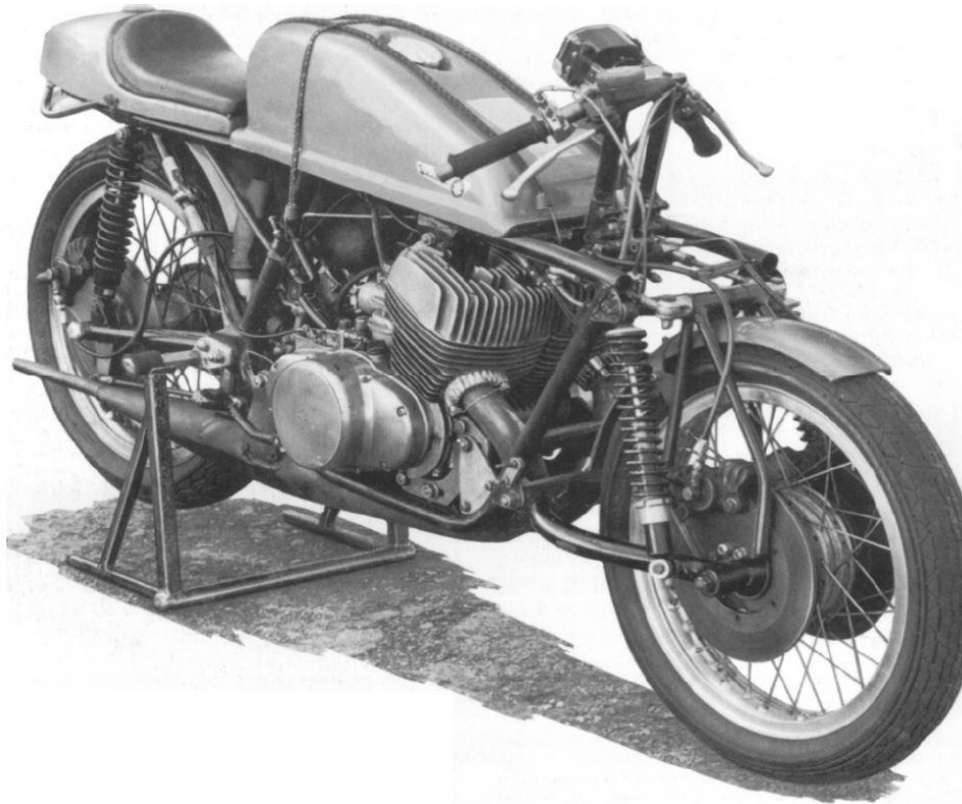


Fig. 1.7 Difazio hub-centre steering on a 500 cc Suzuki-powered racer is shown [2]

Double link

They are mechanically simpler. They comprise of an upright, and the wheel and its bearings are attached to this upright. The upright is kept in place by two pivoted arms that are facing forward, or wishbones, and their front ends allow the suspension movement and steering.

From structural point of view, the several designs in this category differ mainly in the locations on the upright where the two pivoted arms are connected. Considering the lateral stiffness characteristics, this depends only on the stiffness of the wheel and the upright (Fig. 1.8).

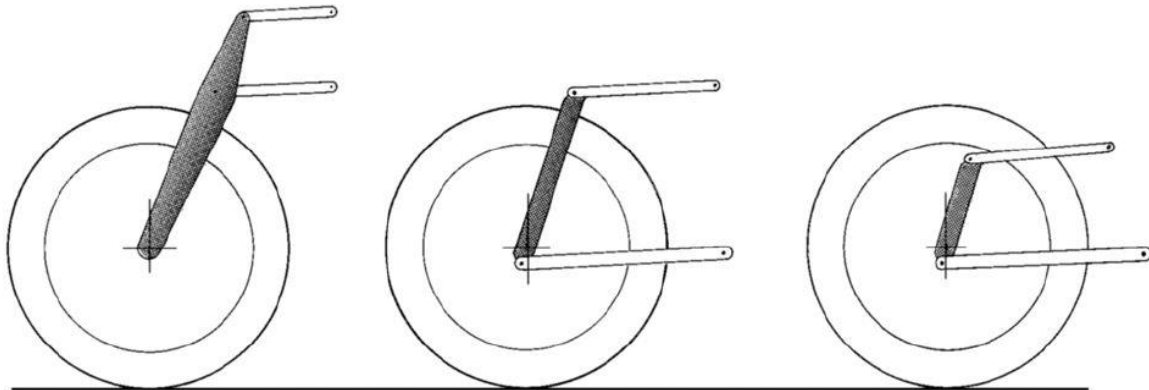


Fig. 1.8 Different types of construction used in double link [2]

Other suspensions in this category are: Elf. E, Hossack/Fior/Foale/Britten (Fig. 1.8a), Foale/Parker/Yamaha GTS, Bump-steer [2].

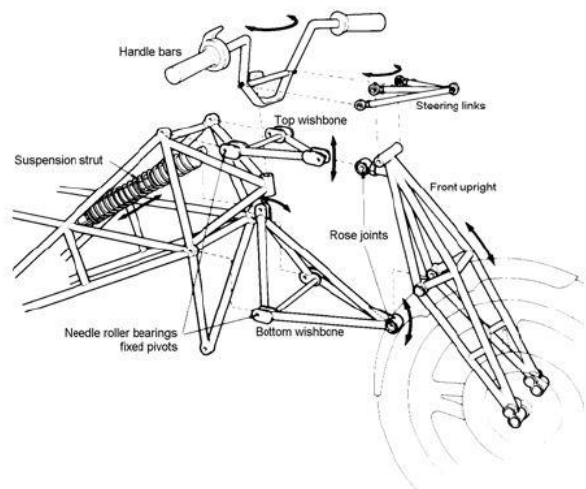
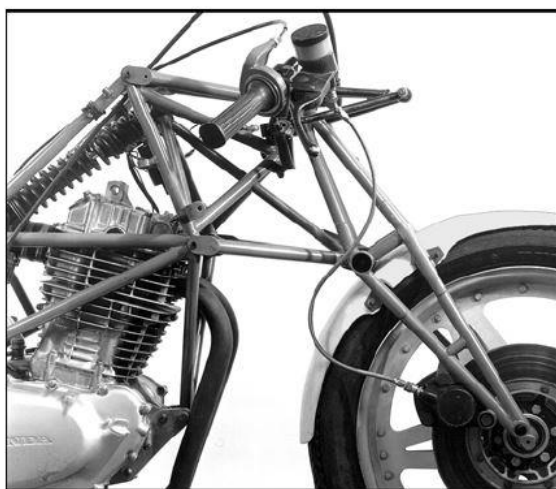


Fig. 1.8a Hossack/Fior/Foale/Britten suspension [2]

McPherson strut based

McPherson strut is widely used in modern street cars, and its main benefits are more related to cost rather than the best technical solution. The wheel in this design is located by strut and rod at the top and by a pivoted link at the bottom. The upper mounting of the spring and the damper rod must be free to allow steering with minimum friction and to rock. The rocking motion is essential because it allows the bottom of the strut to move as defined by the lower pivoted link. It can be observed in the picture below that it seems to combine the drawbacks of the telescopic forks with the link type suspension, without providing any major advantages.

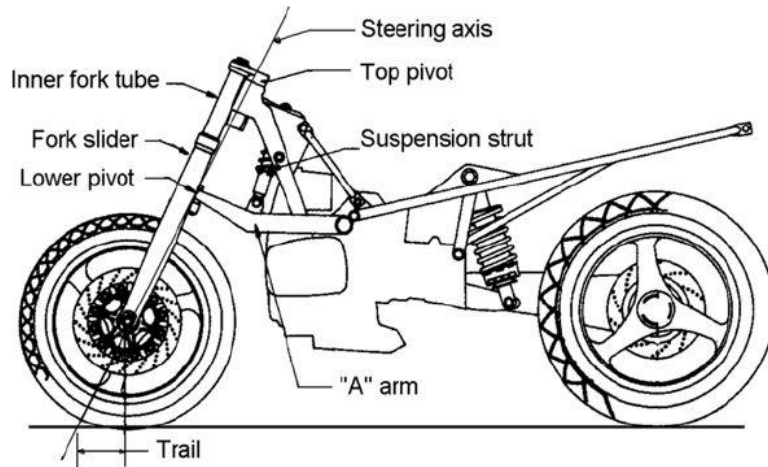


Yet another approach on the Elf bikes (post Cortanze). This design owes much to the McPherson strut, common on modern cars. The typical lower arm is retained but the upper location is done entirely by the suspension unit which has a larger than normal sliding rod.



Fig. 1.9 McPherson strut-based suspension [2]

Some other variants of McPherson strut based suspensions include: Saxon/Motad, BMW Telelever (Fig. 1.9a), Killeen [2].



BMW Telelever. Maybe not in appearance but this type of suspension can be seen as a variant of the McPherson strut. The wheel is mounted to a sliding assembly which is located by a "A" arm.

Fig. 1.9a BMW Telelever [2]

Virtual steering axis

This system is an alternative to the norm because in this system the instantaneous steering axis is defined by the virtual centre of a four-bar linkage. The old OEC motorcycles of the 1920-30s had two such mechanisms, one just below the handlebars and the other one below the axle height. The line passing through the upper and lower virtual centres of these mechanisms was defined as the steering axis. The steering motion was such that as the wheel turned, the steering axis also moved sideways with a small longitudinal movement as well [2].

The components of the four-bar suspension/steering linkage included:

- The wheel axle.
- The main frame of the motorcycle.
- Two side links, or radial arms.

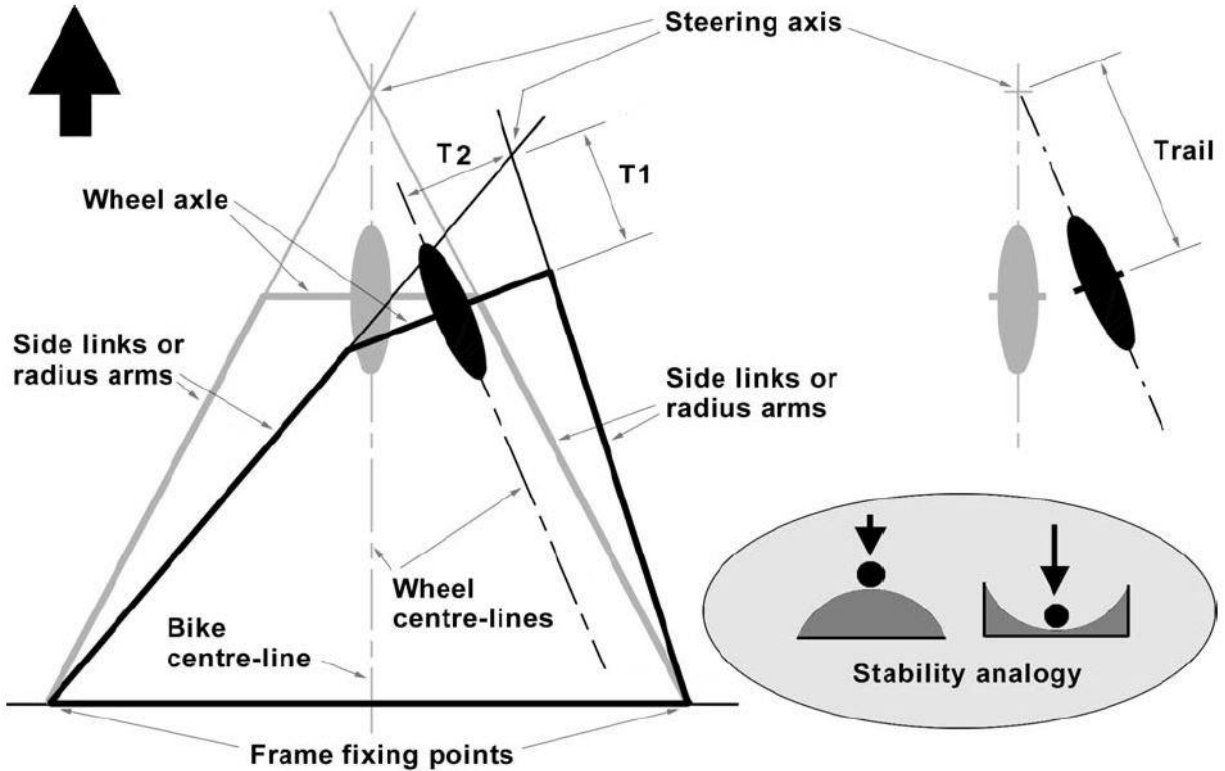


Fig. 1.10 The left sketch represents the system based on virtual steering axis and the right one represents a normal head stock steering design. The ellipses represent tyre contact patches. The grey lines depict the steering in the straight ahead position and the black ones depict it steered to 20 degrees approximately. Both drawings show the projection on the ground. [2]

1.3 Rear Suspension Types

The typical rear suspension consists of a swingarm (a rocker made up of two oscillating arms) with two spring-damper elements, one on both sides (Fig. 1.11a). The main advantages are the reactive forces transmitted to the chassis and the simple construction. The disadvantages are the possibility that the two spring-damper elements generate different forces and therefore torsional stress on the swing arm, and a poorly progressive force-displacement characteristic.

An alternative to the swingarm suspension is the cantilever mono-shock system, which has only one spring-damper unit. However, the positioning of the

spring-shock absorber unit close to the engine can cause problems with the absorber's heat dissipation. Moreover, this suspension does not enable a progressive force-displacement characteristic.

It became easier to obtain the desired stiffness curves with the introduction of four-bar linkage in the rear suspensions. This made possible the selection of different attachment points for the spring-damper elements: for instance, the suspension element is between the chassis and the rocker in the Kawasaki Uni-Trak (Fig. 1.11b), it is between the swingarm and the rocker in Suzuki Full-Floater, and the suspension element is between the swingarm and the connecting rod in the Honda Pro-Link. Large wheel amplitude and modest unsprung masses are obtained, but larger reactive forces are exchanged between the various parts of the four-bar linkage.

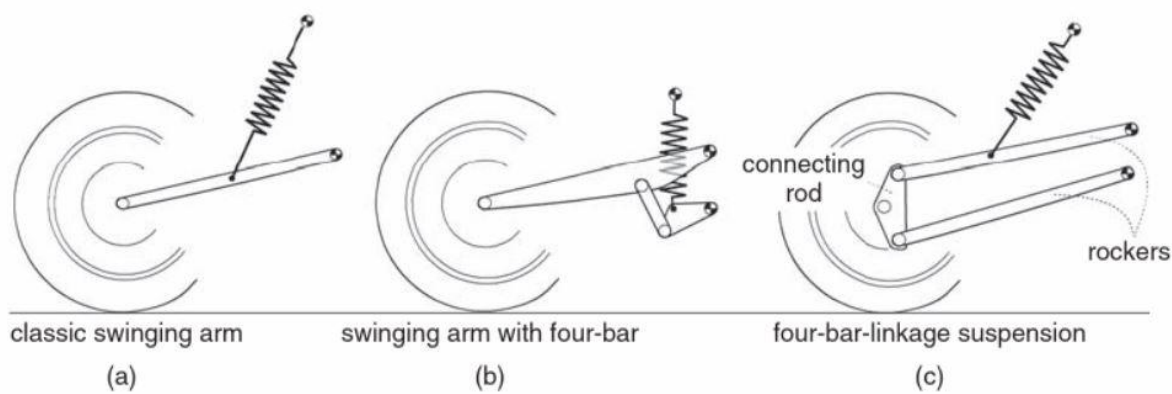


Fig. 1.11 Examples of rear suspensions [1]

The four-bar linkage suspension (Fig. 1.11c) is also the basis for a suspension especially used on the final shaft transmission with universal joints (ex. the BMW Paralever). The wheel is attached to the connecting rod of the four-bar linkage. The suspension act like it is made of a very long fork connected to the chassis at the centre of rotation (the intersection point of the axes of the two rockers). For a proper suspension behaviour, an additional small four-bar linkage

can be added to provide a suitable connection point for the spring- shock absorber element [1].

The French Godier-Genoud endurance racing Kawasaki, in the 1970s, is an example of the link system for racing, which used the pivoted fork triangulated downwards and connected to the suspension strut via a bell-crank. The main aim of these type of designs is to achieve progressive rate springing and damping by geometric means. This method is good in achieving the desired progression, because the springing and damping rates vary together. The design choice depends mainly on the structural and space considerations. The use of minimum number of joints in the system is also quite beneficial.

Basically, all the rear suspensions are some form of swinging arm, but there are single and dual suspension struts, there are single and dual sided swing arms, some include drive shafts whilst others incorporate the pull of chain drive and a wide variety of rocker designs.

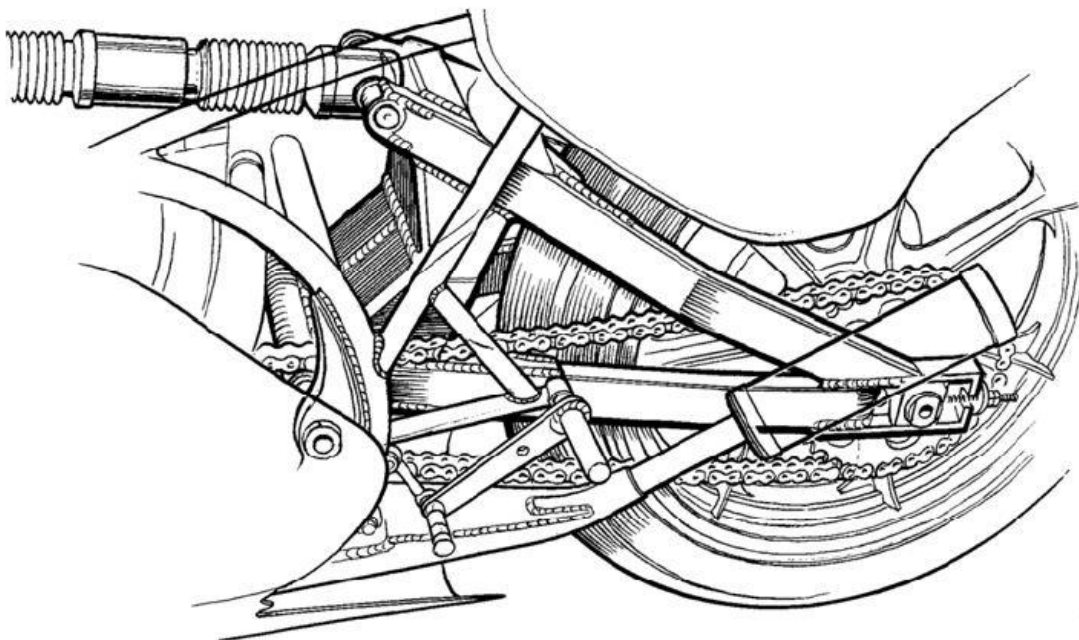


Fig. 1.12 One of the interpretations of the ‘cantilever monoshock’, by Yamaha [2]

A monoshock system was introduced by Yamaha, with a triangulated swing arm and other manufacturers followed with a wide variety of rocker systems, just slightly different in designs to avoid legal problems with a patent by a competitor. But basically, they were not very different. These rocker systems, in addition to just being able to use single suspension units with reduced movements, allow great control over the spring rate properties. Progressive, regressive and their combinations are achieved easily.

Single vs. dual sided

Even though the single sided swing arms have long been used on scooters and small mopeds, the removal of one of the two traditional swing arms became generally considered as a possibility for large racing and sport machines, after the elf sponsored, Cortanze designed endurance racing bikes of the 1970s. It has been used by Honda on many of their sports and racing bikes, both chain and shaft drive, Ducati have succeeded on the racetrack while BMW changed to single sided suspensions exclusively on their shaft drive models, at first with a simple rigid arm and then later with an articulated “paralever” system to control the rise and squat. MV decided to use a cast single sided swing arm suspension on their F4 superbike.

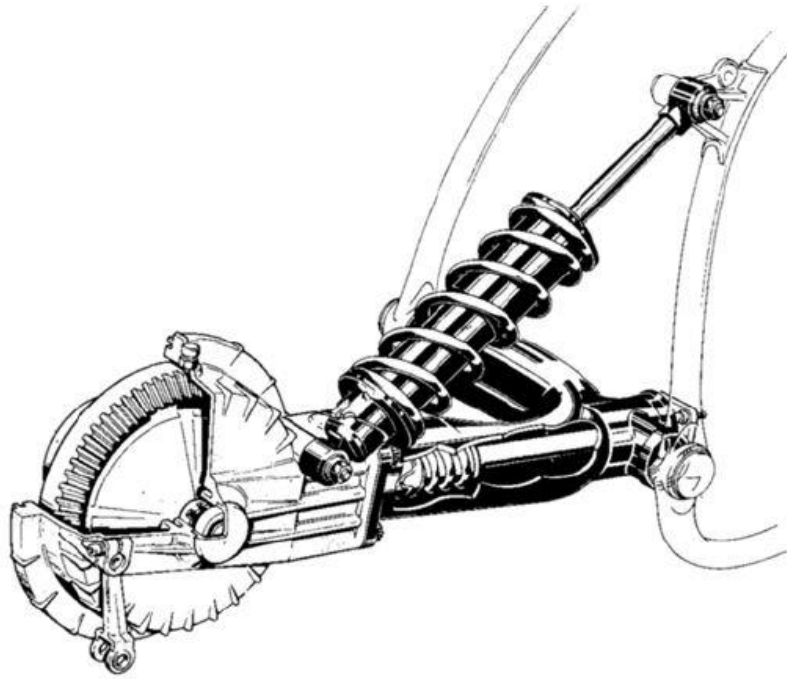


Fig. 1.13a BMW's early version of the single sided swing arm for shaft drive [2]

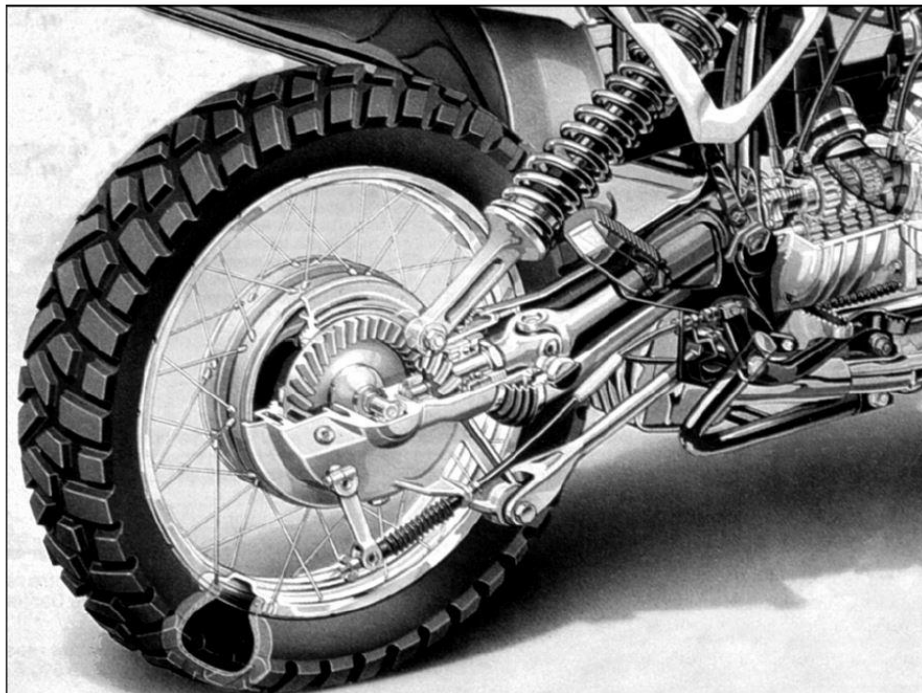


Fig. 1.13b BMW's "paralever", the later model [2]

In terms of the structural stiffness, the double-sided arm with the second cross tube and the single sided arm with gusset have almost equal stiffness against camber change. It can be said that the addition of the gusset to the single sided arm and the second cross tube to the double-sided arm is structurally very efficient. Both types can be made to work equally well depending on the quality of the design details. The ease of wheel changing should be of great advantage for the single sided arms in endurance racing. But other factors like cost, ease of chain adjustments and such have to be taken into account [2].

1.4 Controlled Suspensions

Suspensions can be further categorized on the basis of how the control of the sixth degree of freedom is implemented, which is the degree of freedom controlling the motion of the wheel with respect to the vehicle body.

The suspension systems comprised only of springs and dampers are also known as *passive*, because their energy contributions are entirely negative in response to forces coming from the road. They can only dissipate energy in the form of heat. There is no control either of the spring or the damper. They can only have bilinear characteristics, and during the design stage and the life of the damper, which cannot be changed.

Although passive suspensions provide decent trade-off between handling and comfort, the limitation of these suspensions is evident by the impossibility to manage two independent parameters – body vertical accelerations (related to the comfort) and vertical force variations (related to active safety) – with only one parameter, the damping coefficient of the suspension.

With improved mechanical components and application of microelectronics, passive suspensions have developed into *controlled* or *adaptive* suspensions. They require positive energy from the outside to operate. They are also called *active* suspensions [7].

1.4.1 Semi-active Suspensions

The control bandwidth for these suspensions is in the order of 30-40 Hz. They have a small power request of 10-20 W. The semi-active suspensions allow to have a variation of the damping coefficient both in bounce (compression) and rebound (extension), so they can work in first and third quadrants. These systems have hydraulic devices that work by modifying the section area of the fluid that is passing from one chamber to another.

Variable damping shock absorbers

These are basically types of semi-active suspension systems. In these devices, the area of the orifice can be varied in order to change the force/velocity characteristics of the damper.

A typical *damping actuator* is characterized by two valve holes that can be activated in the active mode in order to change the area of the orifice, and thus the relation between force and velocity.

An accumulator is present for compensating the lack of equality in the volume of fluid passing from one chamber to another.

The *electromagnetic* valve hole is characterized by a solenoid which is a conductive element, so that it can be activated or deactivated. When a power is supplied to the solenoid, a magnetic field is produced.

It is controlling the passage of the fluid by means of air gap between the magnetic field and controlling the motion of the poppet with respect to the vertical axis. Thus, by controlling the current of the electromagnet the vertical movement of the main poppet can be controlled, and so the area of passage of the fluid.

Magnetorheological: In these systems, the fluid modifies its viscosity if there is a magnetic field passing through it. By modifying the viscosity of the fluid, the damping force can be modified. In this case, laminar flow is exploited so that the

pressure drop between the two ends of the controlled chamber is governed by viscosity.

This type of solution had a moderate level of success. This solution is mainly adopted in high segment vehicles or sports cars. The main drawback of the magnetorheological solution is that the particles of materials that are introduced in the fluid, which are sensitive to the variation of the magnetic field, are subject to some aging; therefore, during the life of the device the performance can change.

Electrorheological: In this case, the fluids used are sensible to the voltage drop applied to the fluid. So, applying a difference of potential between the two sides of a chamber (between piston and tube wall), the fluid passing through this area will have a different viscosity. Therefore, regulation of the voltage drop results in the regulation of the damping force applied to the damper.

Not a success in automotive, because voltage needed to have a significant modification are high, so not applicable. Because voltage drops higher than 1 kW are subject to restrictions in the automotive field.

Electromagnetic: In this case, the external resistance can be modified in order to change the damping coefficient and change the relation between force and velocity.

This principle is applicable, but not in a direct mode. Because this one is a linear application in which there is no reduction system between the electromagnetic device and mechanical element which is sliding of one body with respect to the other one. Prototypes made using this principle were bulky and their size and mass was not acceptable.

1.4.2 Active Suspensions

They are mainly of two types:

Slow Active: They work in all four quadrants, because they are active devices. They act in terms of force. These types of devices are implemented mainly to control the roll motion of the vehicle, by acting on the anti-roll bar. They are

mainly for handling performance. The control bandwidth for these systems is in 1-5 Hz and they have a power request of 1-2 kW.

Fully Active: An actuator is installed between the vehicle body and the wheel that can work as force actuator. So, it is able to brake, but also to apply a force between the vehicle body and the unsprung mass so that it can work in all four quadrants (as explicated in Fig. 1.14). In this case, the spring element is no longer present. These systems have control bandwidth in the range of 20-30 Hz and have very high power request of 5-10 kW.

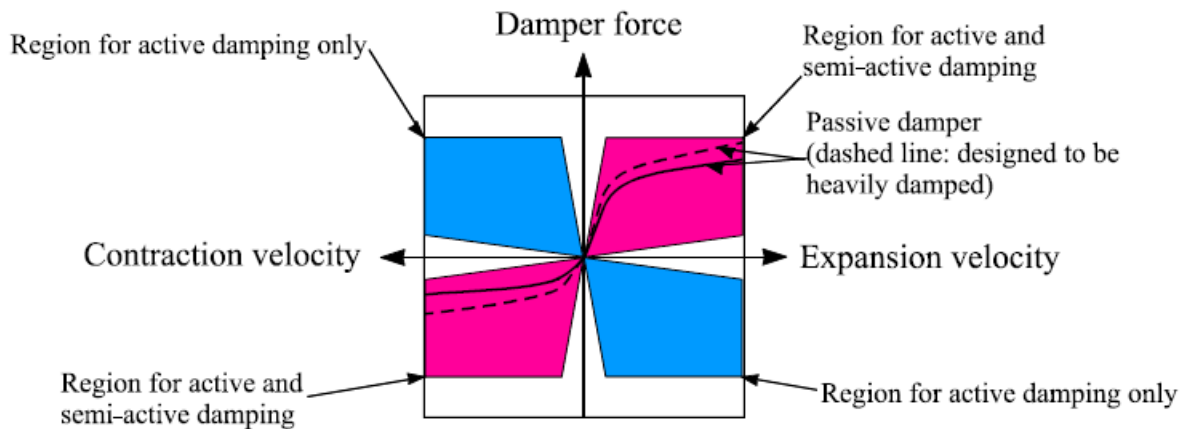


Fig. 1.14 Force–velocity regions for active, semi-active and passive damping. Here, the velocity is the relative speed between the car body and the wheel [8].

1.4.3 Regenerative Shock Absorbers

Due to the use of variable dampers, the suspension systems have seen significant improvements in the last years. Moreover, the gradual increase in the efficiency of the chassis subsystems has led to the use of regenerative shock absorbers, in which electric machines can be used as generators to recover part of the energy. These devices can vary their damping characteristics while converting part of the otherwise wasted energy by the damper into electricity.

The regenerative shock absorber discussed in this project uses an electrohydrostatic transmission to transfer mechanical power between the rotary and linear domains. In these systems, the electric motor is coupled to a fixed-displacement hydraulic pump. The inlets of this pump are connected to the chambers of a linear hydraulic actuator through two lines. Thus, the linear motion of the piston will result in a fluid flow inside the hydraulic circuit, and finally, angular motion of the electric motor will start. The electric machine will be able to vary its damping behaviour, if controlled properly. Furthermore, it can generate electric energy which can be stored in a battery [4].

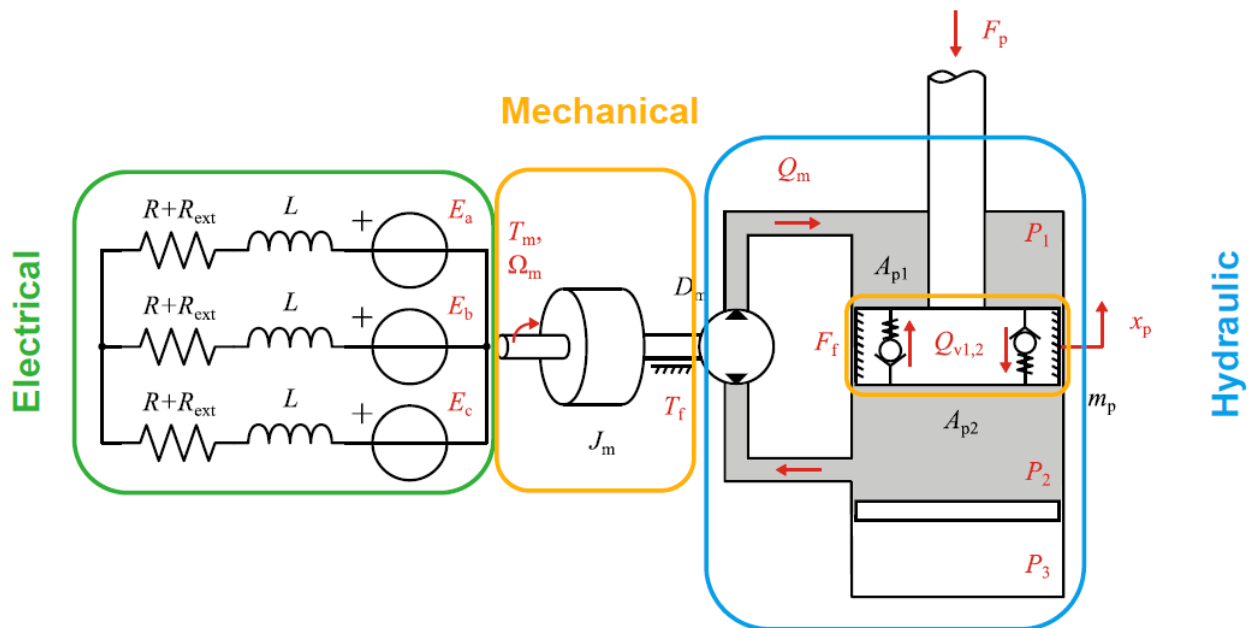


Fig. 1.15a Model scheme of the electrohydrostatic regenerative shock absorber

If pressure in chamber 1 (P_1) becomes higher than the pressure in chamber 2 (P_2), the valve hole is going to open and vice-versa with the other valve hole opening when P_2 becomes higher than P_1 .

When the piston moves down, the fluid flows according to the arrows show in the figure and reach the upper chamber. An accumulator is present to manage the difference of the fluid.

The hydraulic motor is connected to the electric machine by means of a shaft.

In the three-phase motor R_{ext} is controlled to govern the flow of current inside the electric circuit, which means the damping is controlled according to the equation:

$$F = Bli = [(Bl)^2(\frac{1}{R+R_{ext}})].\dot{x}$$

From the three-phase current, we are passing to DC by means of proper electronic device, and this DC current is entering in a battery to be stored.

Therefore, we are not only able to vary the damping by acting on the R_{ext} , but also can recover part of the dissipated energy.

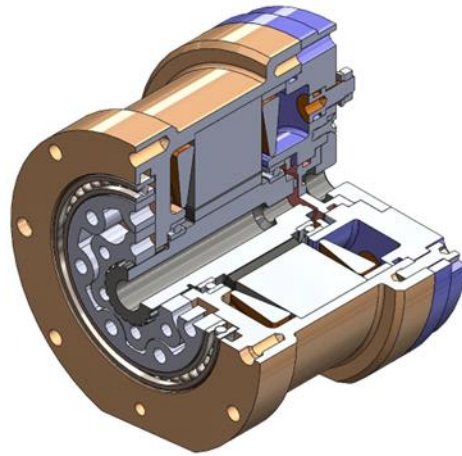


Fig. 1.15b Section view from the prototype of a gerotor pump unit of the electrohydrostatic regenerative shock absorber

1.5 Thesis motivation

The motivation of this thesis project is to study the performance of the damper in dynamic conditions. For this purpose, a Matlab/Simulink model was developed for Electromagnetic Regenerative dampers for motorcycle suspensions. To that end, a mono-corner (quarter car) model was used which represents the front suspension of a motorcycle.

First, an ideal damper model was created. Then to simulate a real passive damper, a lookup table was used. Furthermore, skyhook and groundhook control strategies were implemented to the model and the efficiency map of the motor was also used to account for losses during power evaluation. After trying different combinations of the damping coefficients, finally their simulation results are compared with each other to evaluate the performance in terms of best trade-off between comfort and handling.

1.6 Thesis Outline

This thesis work is organized as follows:

- *Section 2*: It explains the modelling procedure starting with the standard quarter car model. Then the development of quarter car model for ideal and real passive suspension systems is described, along with the Simscape models for comparison. After that, a brief introduction of the *skyhook* and *groundhook* control strategies are given. Following with the quarter car modelling for the real-world *skyhook* and real-world *groundhook* applications is discussed.
- *Section 3*: It mainly deals with the simulation results and the corresponding plots and tables, along with some descriptions. Starting from the ideal quarter car model, then quarter car model with lookup table, and finally quarter car models with active *skyhook* and active *groundhook* control strategies.
- *Section 4*: It presents the final conclusions of this thesis project.

2. Methodology

2.1 Quarter car model

The main excitation source of the vehicle vertical vibrations is coming from the wheels when they follow the irregular road surface with the profile x_0 , as the vehicle travels on the road. The quarter car model is considered to represent the front suspension of a motorcycle, is a standard two degrees of freedom model. Its scheme is shown in the Figure 2.1.

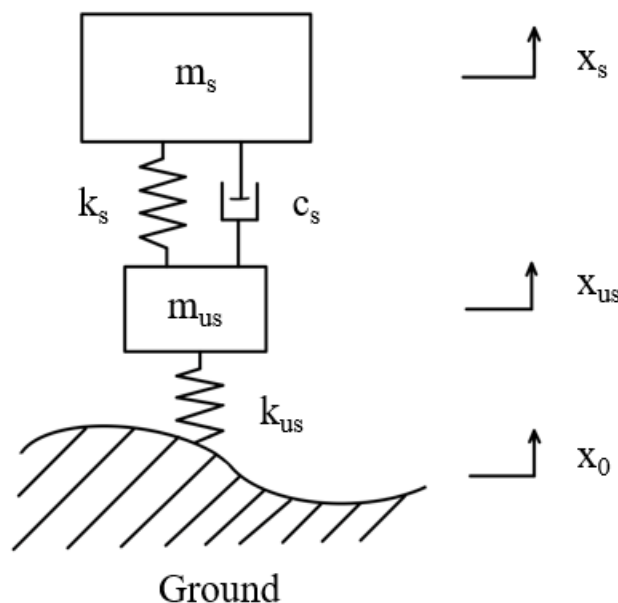


Fig. 2.1 Quarter Car Model with two degrees of freedom

The tire damping is neglected. The other model parameters are reported in the Table 2.1

Sprung mass [kg] $\rightarrow m_s$	119.6
Unsprung mass [kg] $\rightarrow m_{us}$	20
Suspension stiffness [N/m] $\rightarrow k_s$	14000
Tire stiffness [N/m] $\rightarrow k_{us}$	130e3
Suspension damping [Ns/m] $\rightarrow c_s$	2700 (min.) or 5400 (max.)

Table 2.1 Quarter car model parameters for front suspension of a motorcycle

2.1.1 Passive damper

Starting with ideal passive damper and considering the lumped parameters approach and ideal conditions, the equations of motion for the quarter car model are as follows:

$$m_s \ddot{z}_s + c_s(\dot{z}_s - \dot{z}_{us}) + k_s(z_s - z_{us}) = 0$$

$$m_{us} \ddot{z}_{us} + c_s(\dot{z}_{us} - \dot{z}_s) + k_s(z_{us} - z_s) + k_{us}(z_{us} - z_0) = 0$$

These equations of motion were transformed into state space representation with state variables and corresponding matrices A, B, C and D, to be implemented in a Simulink model.

State Space representation:

$$\{x\} = [x_1 \ x_2 \ x_3 \ x_4 \ x_5 \ x_6] = [z_s \ \dot{z}_s \ z_{us} \ \dot{z}_{us} \ \ddot{z}_s \ \ddot{z}_{us}] \text{ states vector}$$

State equations:

- $\dot{x}_1 = x_2$,
- $\dot{x}_2 = -c_s/m_s (x_2-x_4) - k_s/m_s (x_1-x_3)$,
- $\dot{x}_3 = x_4$,
- $\dot{x}_4 = -c_s/m_{us} (x_4-x_2) - k_s/m_{us} (x_3-x_1) - k_{us}/m_{us} (x_3-u)$,
- $\dot{x}_5 = -c_s/m_s (x_2-x_4) - k_s/m_s (x_1-x_3)$,
- $\dot{x}_6 = -c_s/m_{us} (x_4-x_2) - k_s/m_{us} (x_3-x_1) - k_{us}/m_{us} (x_3-u)$

$$\{\dot{x}\} = [A]\{x\} + [B]\{u\}$$

$$\{y\} = [C]\{x\} + [D]\{u\}$$

where x_5 and x_6 represents sprung mass and unsprung mass accelerations respectively.

The resulting matrices are:

$$A = \begin{bmatrix} 0 & 1 & 0 & 0 \\ \frac{-k_s}{m_s} & \frac{-c_s}{m_s} & \frac{-k_s}{m_s} & \frac{c_s}{m_s} \\ 0 & 0 & 0 & 1 \\ \frac{k_s}{m_{us}} & \frac{c_s}{m_{us}} & \frac{-(k_{us}+k_s)}{m_{us}} & \frac{-c_s}{m_{us}} \end{bmatrix}$$

$$B = \begin{bmatrix} 0 \\ 0 \\ 0 \\ \frac{k_{us}}{m_{us}} \end{bmatrix}$$

$$C = \begin{bmatrix} 1 & 0 & 0 & 0 \\ 0 & 1 & 0 & 0 \\ 0 & 0 & 1 & 0 \\ 0 & 0 & 0 & 1 \\ \frac{-k_s}{m_s} & \frac{-c_s}{m_s} & \frac{k_s}{m_s} & \frac{c_s}{m_s} \\ \frac{k_s}{m_{us}} & \frac{c_s}{m_{us}} & \frac{-(k_s+k_{us})}{m_{us}} & \frac{-c_s}{m_{us}} \end{bmatrix}$$

$$D = \begin{bmatrix} 0 \\ 0 \\ 0 \\ 0 \\ \frac{k_{us}}{m_{us}} \end{bmatrix}$$

The Simulink block model is depicted in Figure 2.2

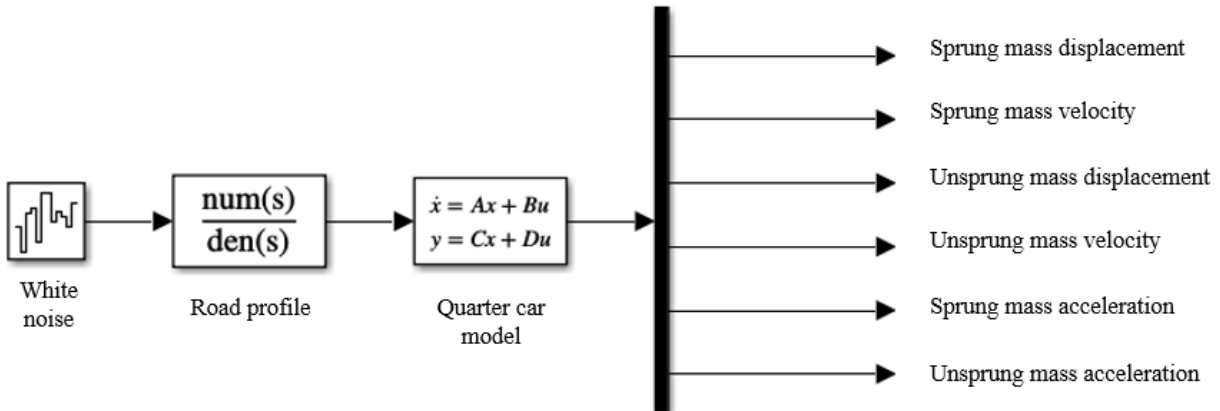


Fig. 2.2 Simulink block scheme of the model

The input to the model is the ground vertical displacement due to road irregularities. To this end, a white noise is used along with a high pass filter, shown in Figure 2.2. We have taken the high pass filter because we are mainly interested in high frequencies, which refer to the road irregularities, that the damping system has to attenuate. The transfer function of the filter is:

$$H = \frac{(2\pi\sqrt{G_r v})s}{s+2\pi f_0}$$

where f_0 is the cut-off frequency of the system, v is the speed of the car G_r is the coefficient of the road-roughness [5].

For evaluating the performance, mainly two parameters are considered: the road holding parameter for handling, and the weighted acceleration of sprung mass for comfort.

Road holding parameter:

For the Road Holding parameter, instead, its computation is based on the actual tire variable vertical force compared to the static vertical force, explained by the equations below:

$$TireForce = k_u(z_{us} - z_{road})$$

$$\frac{\Delta F_{tireRMS}}{F_{z.static}} = \frac{rms[TireForce - k_u \Delta Z_{mus}]}{(m_s + m_{us})g} = \eta_{rh}$$

In which η_{rh} is the Road Holding parameter, k_u is the tire stiffness, the subscript us and s represent the unsprung mass and the sprung mass, respectively, and ΔZ_{mus} is the static vertical displacement affecting the unsprung mass due to the overall weight, defined by:

$$\Delta Z_{mus} = -\frac{(m_s + m_{us})g}{k_u}$$

The resulting expression for the road holding parameter provides useful information regarding the capability of tire in keeping contact with the ground, ensuring different levels of traction and control according to the assumed value: the higher the ratio, the worse the performance of tire-ground contact [6].

Weighted acceleration of sprung mass:

We have used a low order filter according to the ISO 2631 standard, which allows us to compute the weighted acceleration of the sprung mass that accounts for the human sensitivity to acceleration. The transfer function of the filter is:

$$H(s) = \frac{\ddot{x}_w}{\ddot{x}_s} = \frac{80.03s^2 + 989s + 0.02108}{s^3 + 78.92s^2 + 2412s + 5614}$$

We have evaluated the ride comfort as the *rms* value of the acceleration of the vehicle body.

Another important parameter to consider is the power harvesting capability of the suspension, which means the power available to be recovered from the damper by the regenerative system [6].

Harvested Power:

The maximum energy available for harvesting is the energy dissipated by the viscous damping c_s . The instant power dissipated is given as follows:

$$P = c_s (\dot{x}_s - \dot{x}_{us})^2$$

We focus on the average power and not the rms value of the power since the average power is proportional to the mean square of the suspension velocity [5].

Road roughness:

The road roughness coefficients for different classes of road suggested by ISO and different velocities used in the model are reported in Table 2.2 and Table 2.3, respectively.

Road class	Road roughness coefficient (Gr)
A (Very good)	1.6e-7
B (Good)	6.4e-7
C (Average)	2.56e-6
D (Poor)	1.02e-5

Table 2.2 Road roughness coefficient

Velocity	[m/s]
V_1	8.33 (30 km/h)
V_2	13.89 (50 km/h)
V_3	19.44 (70 km/h)

Table 2.3 Velocities

Simscape model

To compare and further validate the theoretical quarter car model of the Simulink, a Simscape model was developed. Simscape enables one to rapidly create models of physical systems within the Simulink environment. With Simscape one can build physical component models based on physical connections that directly integrate with block diagrams and other modeling paradigms. The scheme of the Simscape model is depicted in Fig. 2.3.

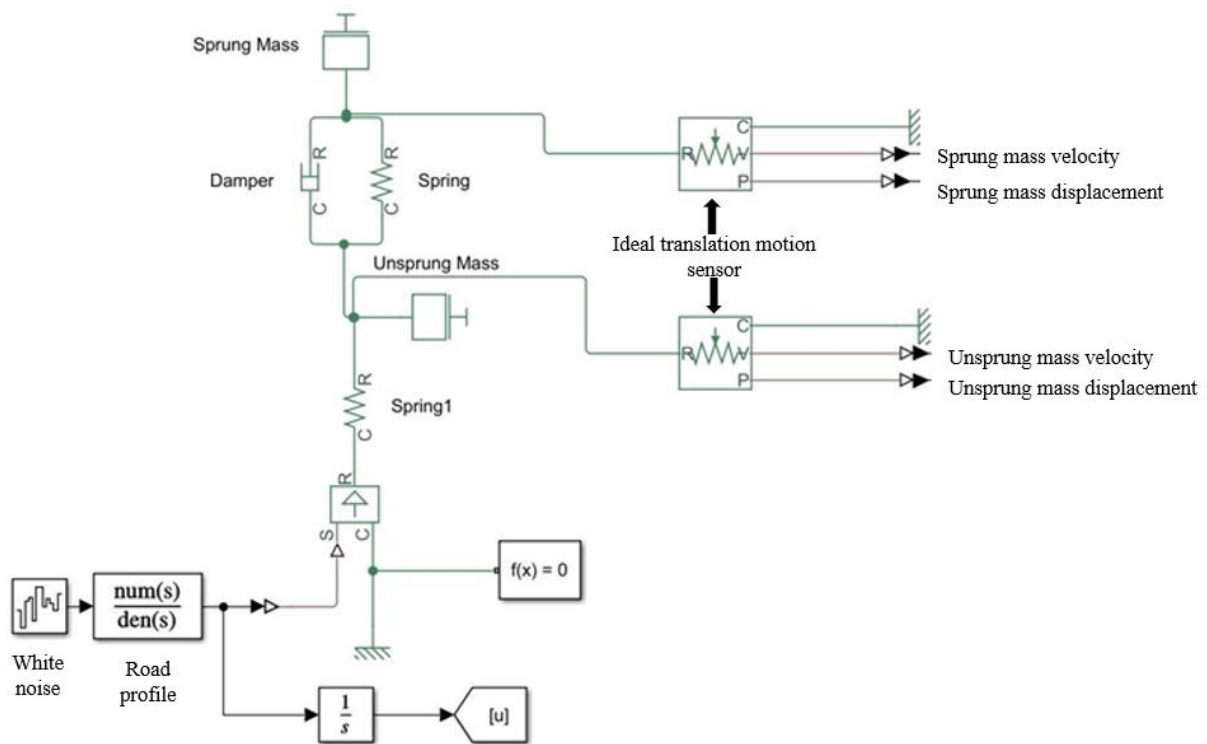


Fig. 2.3 Simscape model scheme

In the development of the Simscape model, blocks from the Simscape library are used which represents physical elements like the damper, spring, sprung mass, unsprung mass etc., which can be linked to the Matlab program via proper codes. The model also incorporates blocks from the Simulink environment. In addition to that, two *Ideal translation motion sensors* were used to extract velocities and displacements of the sprung and the unsprung masses.

2.1.2 Real passive damper

For simulating a passive damper in real dynamic conditions, instead of using a constant damping coefficient, a force-velocity characteristic obtained from experimental results, was introduced in the form of a lookup table to the Simulink model. This lookup table provides the damping characteristics to our model by taking input as velocity and giving the output as the damping force.

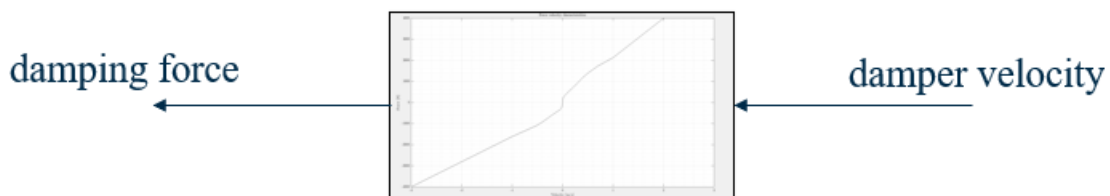


Fig. 2.4 Force-velocity characteristic (lookup table)

The damping characteristic provided by the lookup table is a good approximation of the constant linear trend of the Force-velocity curve in the ideal case. The corresponding quarter car representation is depicted in Fig. 2.5.

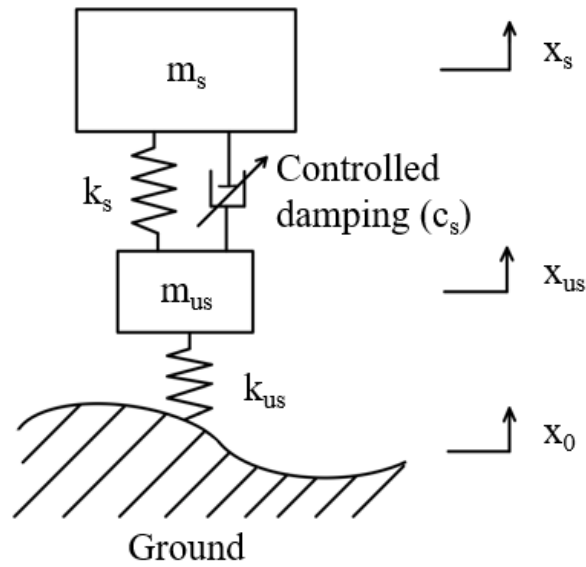


Fig. 2.5 Quarter car model with a controlled damper

Instead of one input in the ideal case, now there are two inputs, namely, the road irregularities and the damping force provided by the force-velocity characteristic. These two inputs are entered in the quarter car model in the Simulink. The relevant Simulink block scheme is shown in Fig. 2.6. Rest of the model is developed as the previous ideal damper model.

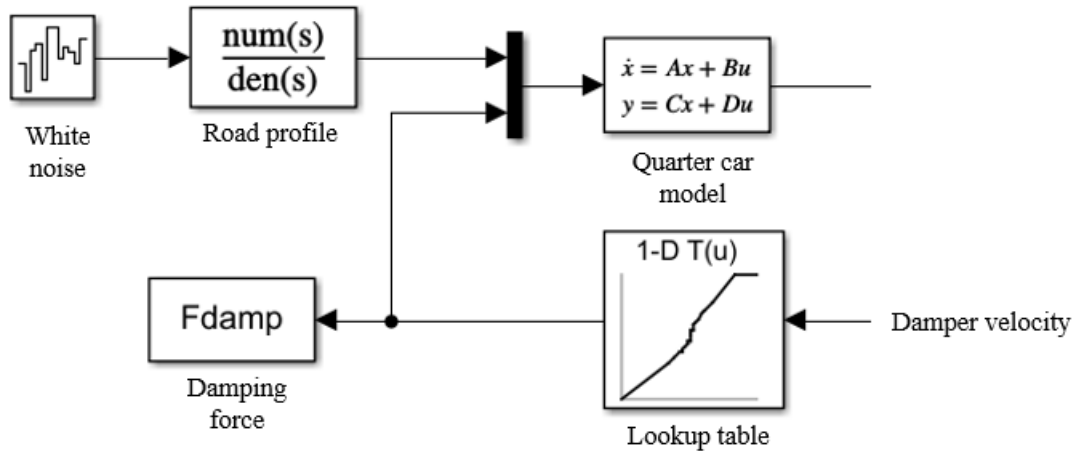


Fig. 2.6 Passive damper with the lookup table

Real Simscape model

Again, a Simscape model was developed to compare and validate the theoretical quarter car model of real passive suspension developed in Simulink. The block scheme of the Simscape model with lookup table is shown in the Fig. 2.7.

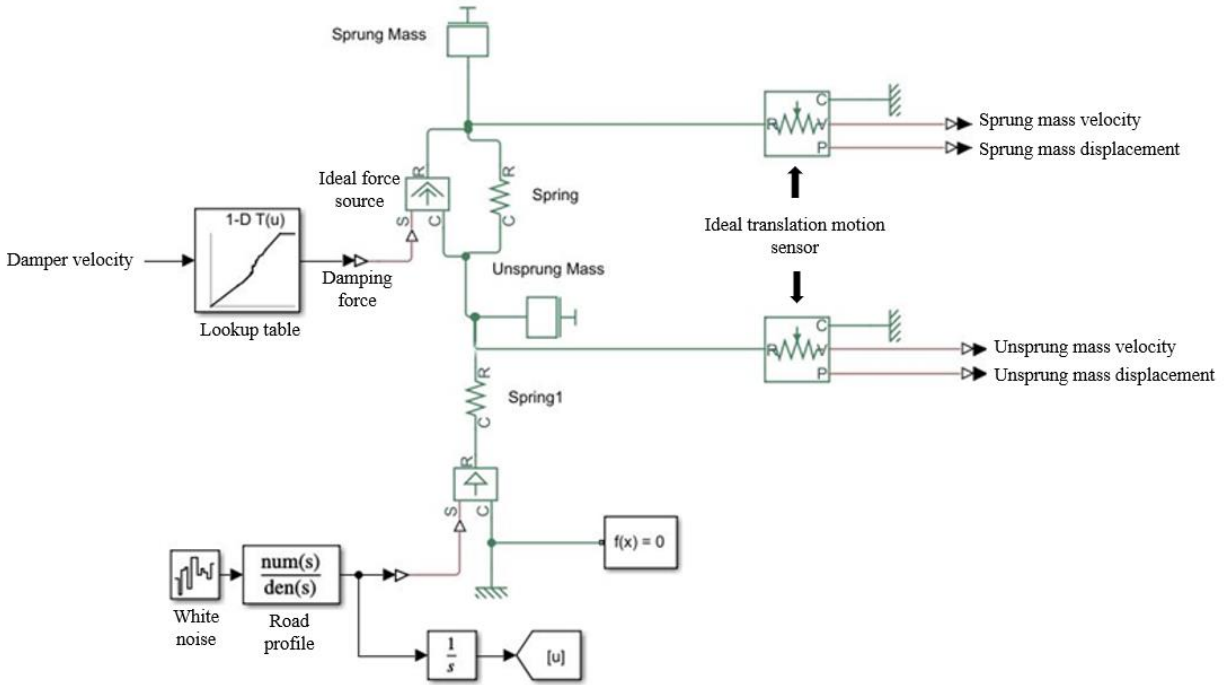


Fig. 2.7 Simscape model with lookup table

The modelling procedure is same as the previous Simscape model for the ideal passive damper model, with an addition of the lookup table, which takes as input the damper velocity and gives the damping force. Furthermore, an *Ideal Force Source* block is used to replace the conventional damper. This block represents an ideal source of force that generates force proportional to the input physical signal. The block connections R and C are mechanical translational conserving ports. Port S is the physical signal port, through which control signal that drives the source is applied.

2.2 Control Strategies

For the next part of this project, some active control strategies were implemented to the model in order to evaluate the performance of the actuator system. For this purpose, the *Skyhook* and *Groundhook* control strategies were used.

The lookup table from the previous model is replaced by the efficiency maps of the motor pump unit to account for the losses and also for torque computation.

Because in reality, the actual damping force is lower than the requested damping force due to losses. Also, the force exerted by the actuator is introduced in the equations of motion, as well as in the Simulink model, by means of the Matlab function block.

2.2.1 Skyhook control

In the ideal *skyhook* model, a standard quarter car model with two degrees of freedom is used. The only difference is that in the *skyhook* the damper is not situated between the two masses, but between the sprung mass and a fixed point to damp the vehicle body motion in an optimal way. The damper is attached to a point fixed in the inertial frame (chassis). The damper (c_s) substitutes the conventional shock absorber, while it is added to the model if the conventional shock absorber (c) between the two masses is still present. The corresponding *skyhook* models without and with the conventional shock absorber are shown in Fig. 2.8.

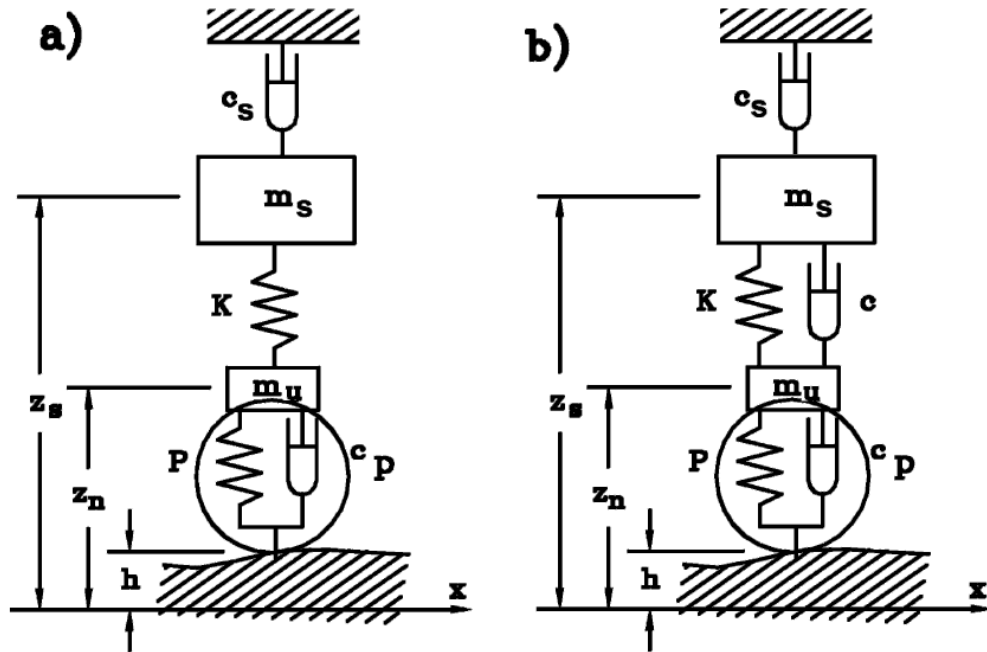


Fig. 2.8 a) Ideal *skyhook* without the conventional shock absorber, b) with the conventional shock absorber [3]

For the real-world application, the fixed point where the *skyhook* is attached does not exist. This strategy must be implemented using a semi-active damper with a controllable damping coefficient, located between the two masses. The controlled damper must supply a force

$$F = -c_s \dot{z}_s - c (\dot{z}_s - \dot{z}_{us})$$

The *skyhook* model with a semi-active solution for real-world application is depicted in Fig. 2.9.

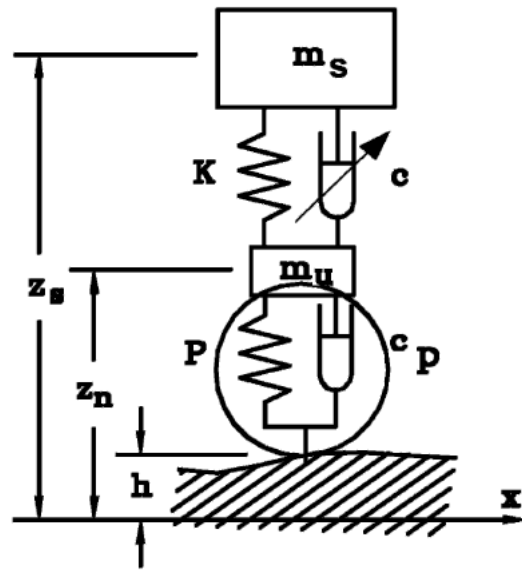


Fig. 2.9 Skyhook with semi-active damper for real-world application [3]

Active system quarter car with real-world skyhook

This project focuses on the implementation of such an active control strategy. For an active system, a device which is able to operate on all four quadrants of the force-velocity characteristic of the damper, and which can transfer energy to the system is considered. The conditions in which a passive system operates lie in the second and fourth quadrants, where force and velocity have opposite signs. While an active system can also exert forces with the same sign of the velocity, thus it is able to work in all the four quadrants of the force-velocity plot. The scheme of this type of model with a controlled actuator which replaces the controlled damper of the semi-active solution in the previous case, is depicted in Fig. 2.10.

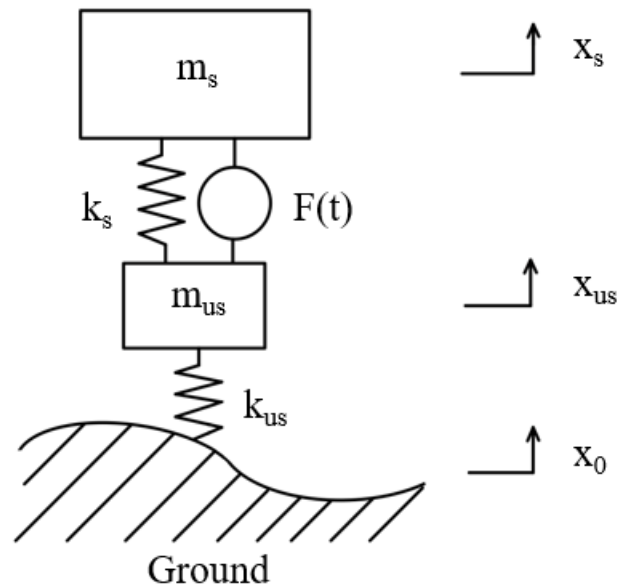


Fig. 2.10 Active *skyhook* model with a controlled actuator supplying all the force exerted between the sprung and unsprung masses

Neglecting the damping of the tires, the equations of motion are:

$$m_s \ddot{z}_s - F + k_s(z_s - z_{us}) = 0$$

$$m_{us} \ddot{z}_{us} + F - k_s(z_s - z_{us}) - k_{us}(z_0 - z_u) = 0$$

where z_0 is the road surface irregularity, F is the force exerted by the actuator on the sprung mass.

As mentioned earlier, the efficiency map of the motor pump unit is implemented in the Simulink model to account for losses and also for the torque computations. At first, the lookup table from the previous model, which provides damping from experimental results, was used as an input along with the damper velocity to the motor efficiency block. Then the output from this block, which is the actual damping force, was compared with the damping force provided by the lookup table. As expected, the actual damping force was lower than the damping force

provided by the lookup table, after the considering the efficiency map of the motor. So, the model was working well.

Furthermore, the force equation representing the force exerted by the actuator between the two masses is also introduced in the equations of motion as well as in the Matlab and Simulink model. For using the force equation, the Matlab function block in the Simulink environment is used. This force equation of the actuator replaces the lookup table used in the previous model for the real passive damper. The force equation indicating the force exerted by the actuator is same as the ideal skyhook model mentioned earlier.

where c_s and c are the damping coefficient of the *skyhook* and the damper, respectively. The force must be according to the above equation in order to simulate the *skyhook* [3].

The equations of motion and the force equation were then converted into state space representation to be used in the Matlab and Simulink environment.

State Space representation:

$$\{x\} = [x_1 \ x_2 \ x_3 \ x_4] = [z_s \ z_{us} \ \dot{z}_s \ \dot{z}_{us}] \rightarrow \text{states vector}$$

$$\{u\} = [x_0 \ F] \rightarrow \text{input}$$

State equations:

- $\dot{z}_s = x_3,$
- $\dot{z}_{us} = x_4,$
- $\ddot{z}_s = F/m_s - k_s x_1/m_s + k_s x_2/m_s,$
- $\ddot{z}_{us} = -F/m_{us} + k_s x_1/m_{us} - (k_s + k_t)/m_{us} + k_{us} x_0/m_{us},$

$$\{\dot{x}\} = [A]\{x\} + [B]\{u\}$$

$$\{y\} = [C]\{x\} + [D]\{u\}$$

$$\{y\} = [z_s \ z_{us} \ \dot{z}_s \ \dot{z}_{us} \ \ddot{z}_s \ \ddot{z}_{us}] \rightarrow \text{output}$$

The resulting matrices are:

$$A = \begin{bmatrix} 0 & 0 & 1 & 0 \\ 0 & 0 & 0 & 1 \\ \frac{-k_s}{m_s} & \frac{k_s}{m_s} & 0 & 0 \\ \frac{k_s}{m_{us}} & \frac{-(k_s+k_{us})}{m_{us}} & 0 & 0 \end{bmatrix}$$

$$B = \begin{bmatrix} 0 & 0 \\ 0 & 0 \\ 0 & \frac{1}{m_{us}} \\ \frac{k_{us}}{m_{us}} & \frac{-1}{m_{us}} \end{bmatrix}$$

$$C = \begin{bmatrix} 1 & 0 & 0 & 0 \\ 0 & 1 & 0 & 0 \\ 0 & 0 & 1 & 0 \\ 0 & 0 & 0 & 1 \\ \frac{-k_s}{m_s} & \frac{k_s}{m_s} & 0 & 0 \\ \frac{k_s}{m_{us}} & \frac{-(k_{us}+k_s)}{m_{us}} & 0 & 0 \end{bmatrix}$$

$$D = \begin{bmatrix} 0 & 0 \\ 0 & 0 \\ 0 & 0 \\ 0 & 0 \\ 0 & \frac{1}{m_{us}} \\ \frac{k_{us}}{m_{us}} & \frac{-1}{m_{us}} \end{bmatrix}$$

As mentioned earlier, the efficiency map of the motor pump unit is implemented in the Simulink model to account for losses. At first, the lookup table from the previous model, which provides damping from experimental results, was used as an input along with the damper velocity to the motor efficiency block. Then the output from this block, which is the actual damping force, was compared with the damping force provided by the lookup table. As expected, the actual damping force was lower than the damping force provided by the lookup table, after the considering the efficiency map of the motor. So, the model was working well.

Furthermore, the force equation representing the force exerted by the actuator between the two masses is also introduced in the equations of motion as well as in the Matlab and Simulink model. For using the force equation, the Matlab function block in the Simulink environment is used. This force equation of the actuator replaces the lookup table used in the previous model for the real passive damper.

The block scheme of the model with the efficiency map of the motor and the force equation of the actuator is given in Fig. 2.11.

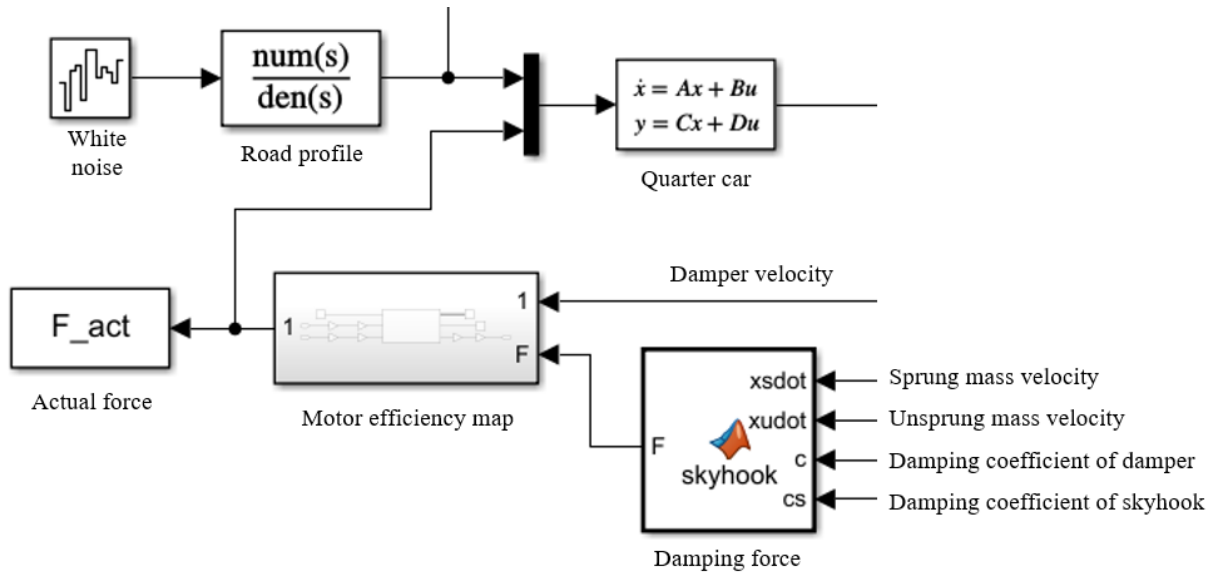


Fig. 2.11 Block scheme of the model with motor efficiency map and actuator force

The block for the motor efficiency map takes as inputs the damper velocity and the damping force given by the force equation of the actuator, and it gives as output the actual damping force. This actual damping force will now enter as input in the quarter car model along with road profile.

The Matlab function block used for introducing the force equation receives as input the sprung and unsprung mass velocities, and the damping coefficient of the damper (c) as well as the damping coefficient of the *skyhook* (c_s); and the output is the damping force exerted by the actuator.

After the modelling, different combinations of the damping coefficients c and c_s were iterated to find the optimum results, which will be reported and discussed in the next section.

2.2.2 Groundhook control

The main idea behind the introduction of the *skyhook* concept was to reduce the vertical accelerations of the sprung mass, without any consideration regarding the unsprung mass. So, the motion of the unsprung mass is quite large, and the corresponding variations of the force on the ground are not acceptable. The variable component of the vertical force on the ground may be approximated by neglecting the damping of the tire

$$F_z = -P(z_{us} - h)$$

In the frequency response in terms of tire-ground force on the quarter car model, there is a significant improvement at low frequency, but things become much worse at high frequency.

The stiffness of the tire or the deformation ($z_{us} - h$) must be reduced in order to minimize the variable component of the force on the ground. To reduce the deformation, a damper may ideally be introduced between the unsprung mass and the contact point with the ground, as depicted in the Fig. 2.12. This approach is usually referred to as *groundhook*.

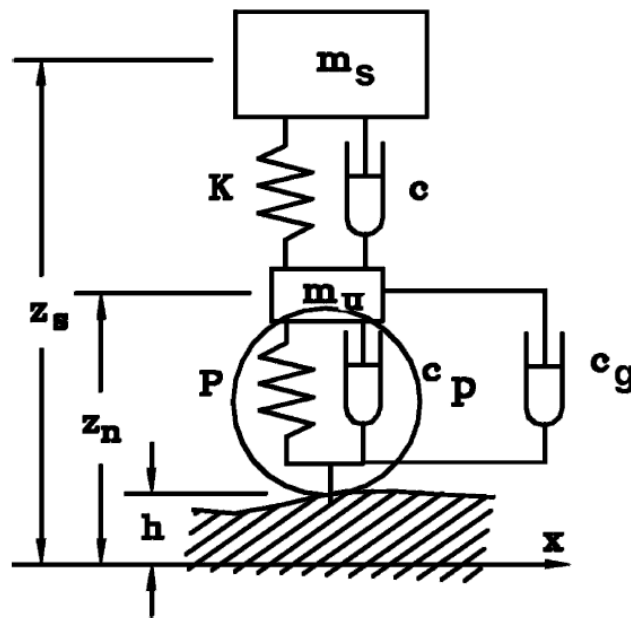


Fig. 2.12 Ideal *groundhook* with a damper located between the unsprung mass and the contact point with the ground [3]

Active system quarter car with real-world *groundhook*

The previous approach was ideal. But to realize this approach, an active device located between the two masses can be used, which is able to work on all four quadrants of the force-velocity characteristic as well as supply all the forces between the two masses. The scheme of such a model using an active system is same as the active skyhook model which is depicted in the Fig. 2.10.

Then the equations of motion of the system are:

$$m_s \ddot{z}_s - F + k_s(z_s - z_{us}) = 0$$

$$m_{us} \ddot{z}_{us} + F - k_s(z_s - z_{us}) - k_{us}(z_0 - z_u) = 0$$

where F is the force exerted by the actuator on the sprung mass, and it is:

$$F = c_g \dot{z}_s - c (\dot{z}_s - \dot{z}_{us})$$

where c_g and c are the damping coefficient of the *groundhook* and the damper, respectively. The force must be according to the above equation in order to simulate the *groundhook* [3].

The equations of motion and the force equation were then converted into state space representation to be used in the Matlab and Simulink environment. The resulting matrices were same as in the previous real-world *skyhook* model, with only difference being the force exerted by the actuator and its corresponding equation.

Again, as in the previous model with active *skyhook*, the efficiency map of the motor as well as the force equation of the actuator were implemented. The rest of the modelling procedure remains basically the same, only the force equation of the actuator is different in this case.

After the modelling is complete, again different combinations of the damping coefficients c and c_g were iterated to find the optimum results, which will be reported and discussed in the next section.

3. Simulations and Results Analysis

3.1 Ideal Quarter Car model

Road holding parameter

The road holding parameter is computed as a rms value for a better comparison. First, the simulation results are analysed by comparing the road holding parameter in different conditions.

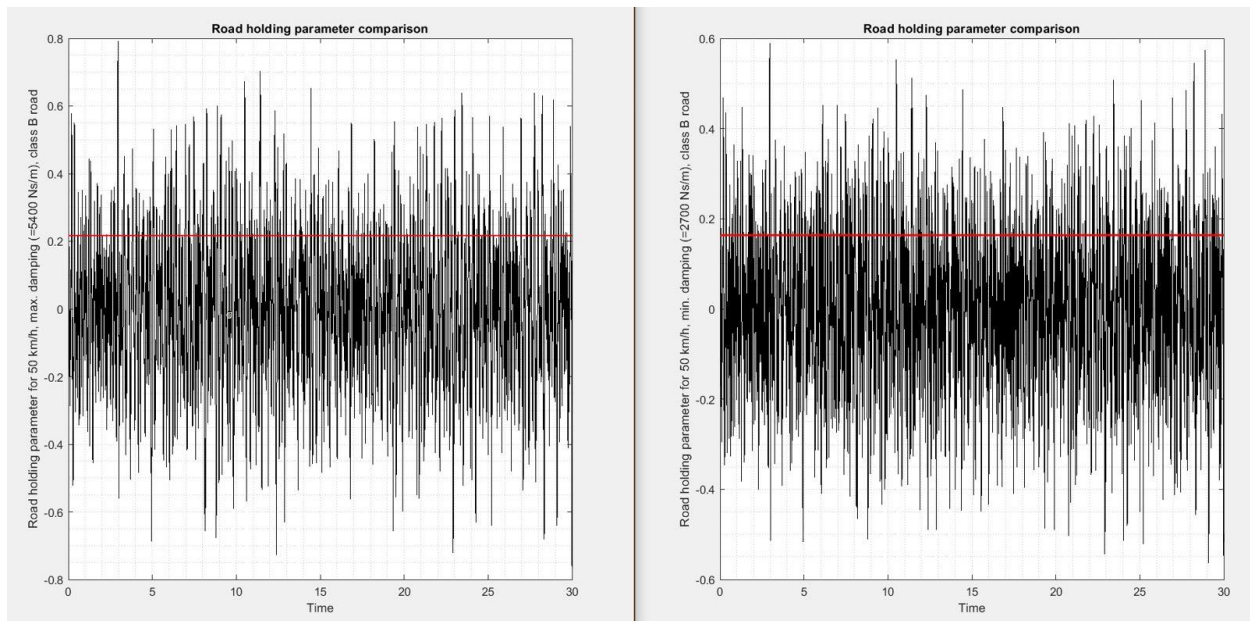


Fig. 3.1 Road holding parameter comparison for different damping coefficients

In Fig. 3.1, the plots show the simulation results by keeping same velocity at 50 km/h and same road grade B (good). Only the damping coefficient is changed. It can be noticed that the road holding parameter decreases when we decrease the damping coefficient. In both the cases, the rms value of the road holding parameter

is around 0.2, which is very good. Because the lower the value of the road holding coefficient, the better is the adhesion of the tire with the ground.

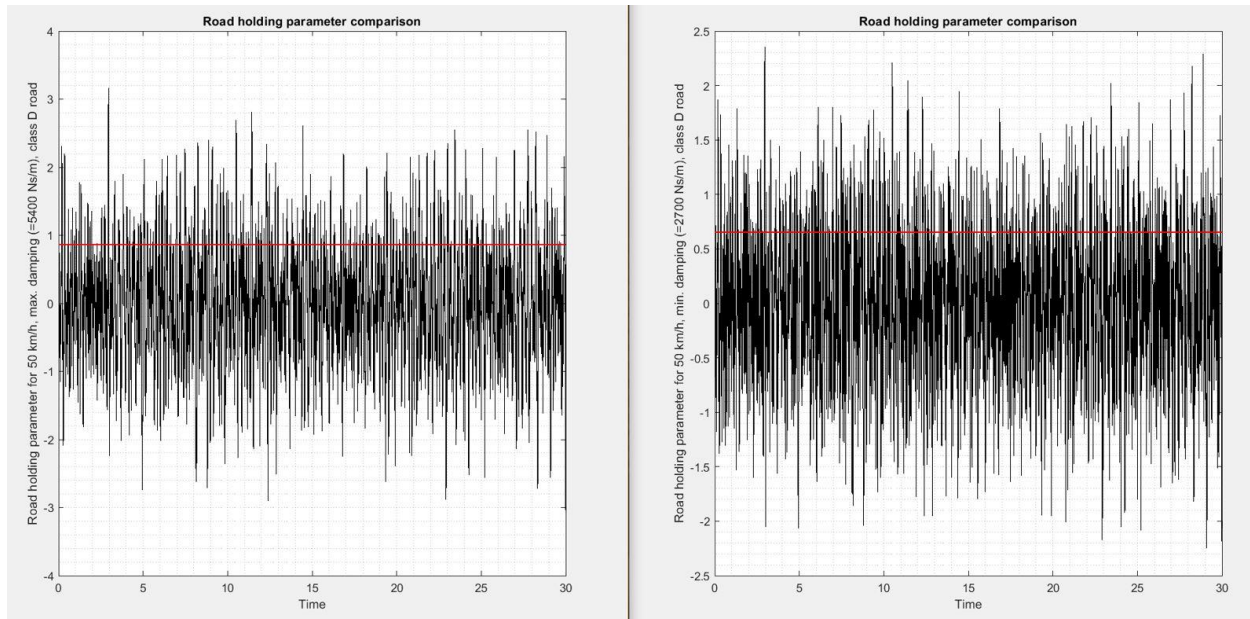


Fig. 3.2 Road holding parameter comparison for different road grade

For the next simulation, only the road grade was changed from grade B (good) to grade D (poor). And everything was kept similar to the previous simulation. The results are demonstrated in Fig. 3.2. Again, the road holding parameter decreases as the damping coefficient decreases. But the important point to notice is that there is an increment in the overall rms value of road holding parameter, as we changed to road grade D (poor), which has higher road surface irregularities. In this case as well, the road holding parameter is below unity, so the wheel will remain in contact with the ground.

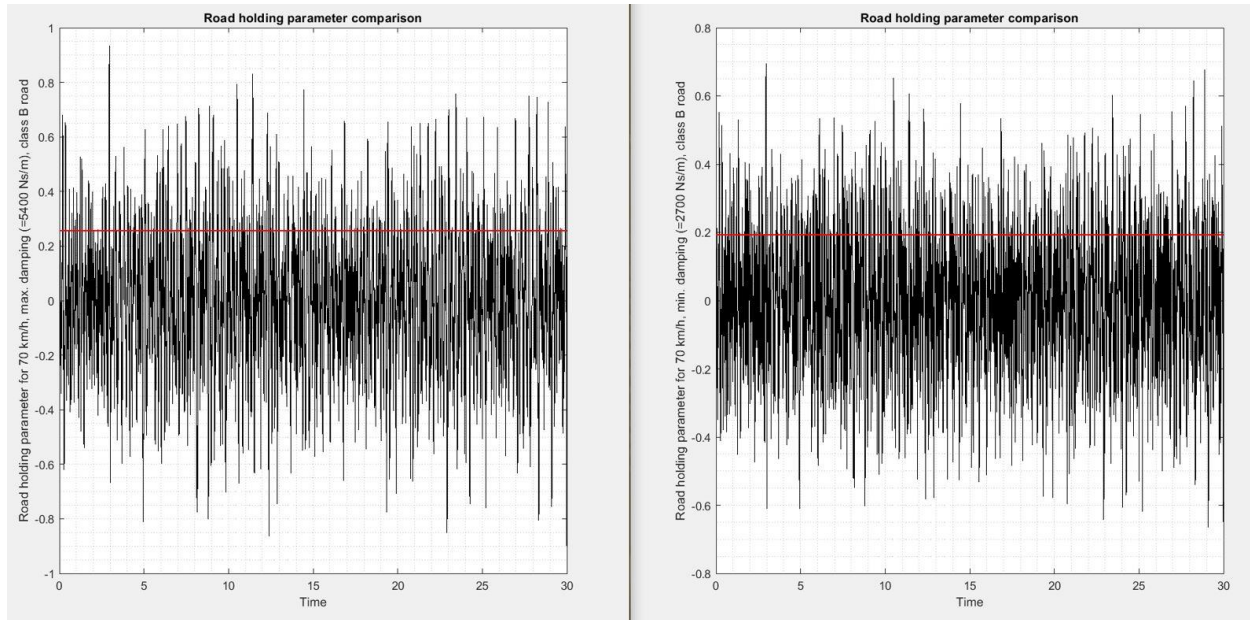


Fig. 3.3 Road holding parameter comparison for different velocity

Similarly, the next set of simulations were performed. This time changing the velocity from 50 km/h to 70 km/h. As it is evident from the Fig. 3.2, by increasing the velocity, the value of the road holding parameter is slightly increased overall. And the value is further increased when we lower the road grade (from B to D). But here also, the value of the road holding parameter is below 1. So, the wheel remains in contact with the ground.

Weighted sprung mass acceleration

For performance analysis in terms of ride comfort, a low pass filter according to the ISO 2631 standard is considered, which allows us to compute the weighted acceleration of the sprung mass that accounts for the human sensitivity to acceleration.

The ride comfort is evaluated as the RMS value of the acceleration of the vehicle body.

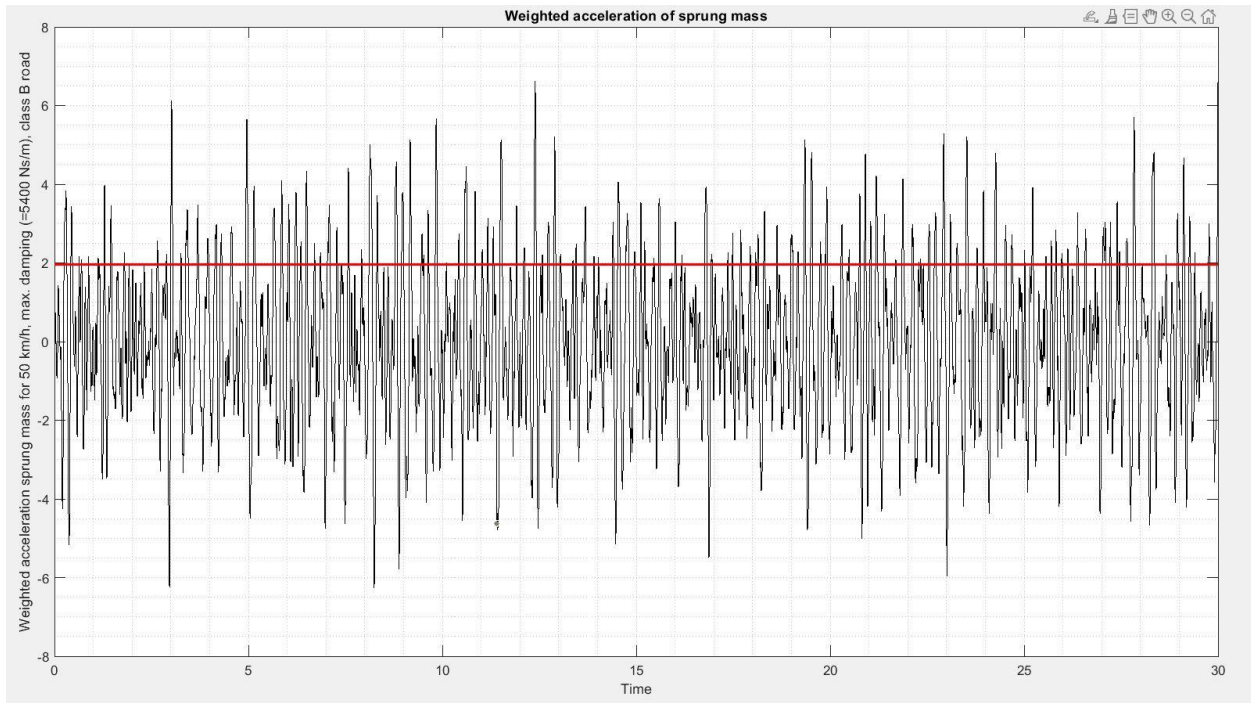


Fig. 3.4a Weighted sprung mass acceleration at $c = 5400$ Ns/m

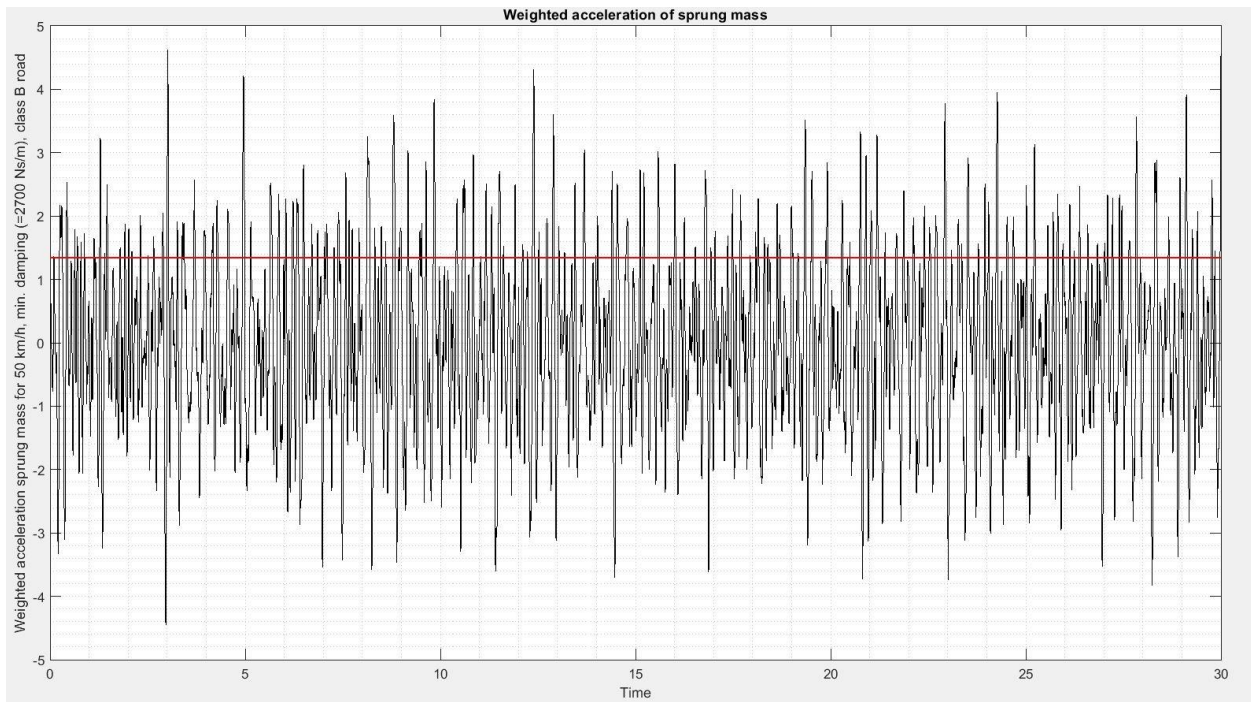


Fig. 3.4b Weighted sprung mass acceleration at $c = 2700$ Ns/m

For the first simulation regarding the weighted sprung mass, the velocity was kept at 50 km/h and the road grade was selected as B. Only the damping coefficient was changed to observe the behaviour of the model. From Fig. 3.4a and Fig.3.4b, a decrement of the weighted sprung mass acceleration rms value is noted when the damping coefficient was decreased.

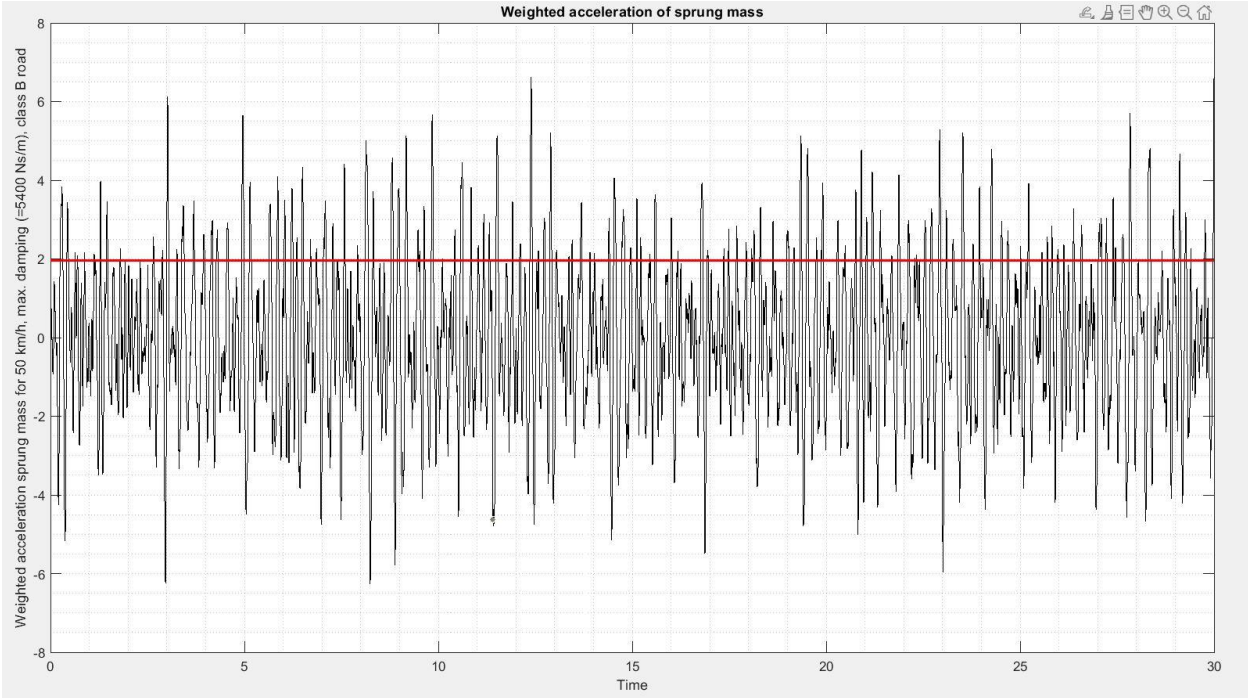


Fig. 3.5a Weighted sprung mass acceleration at road grade B

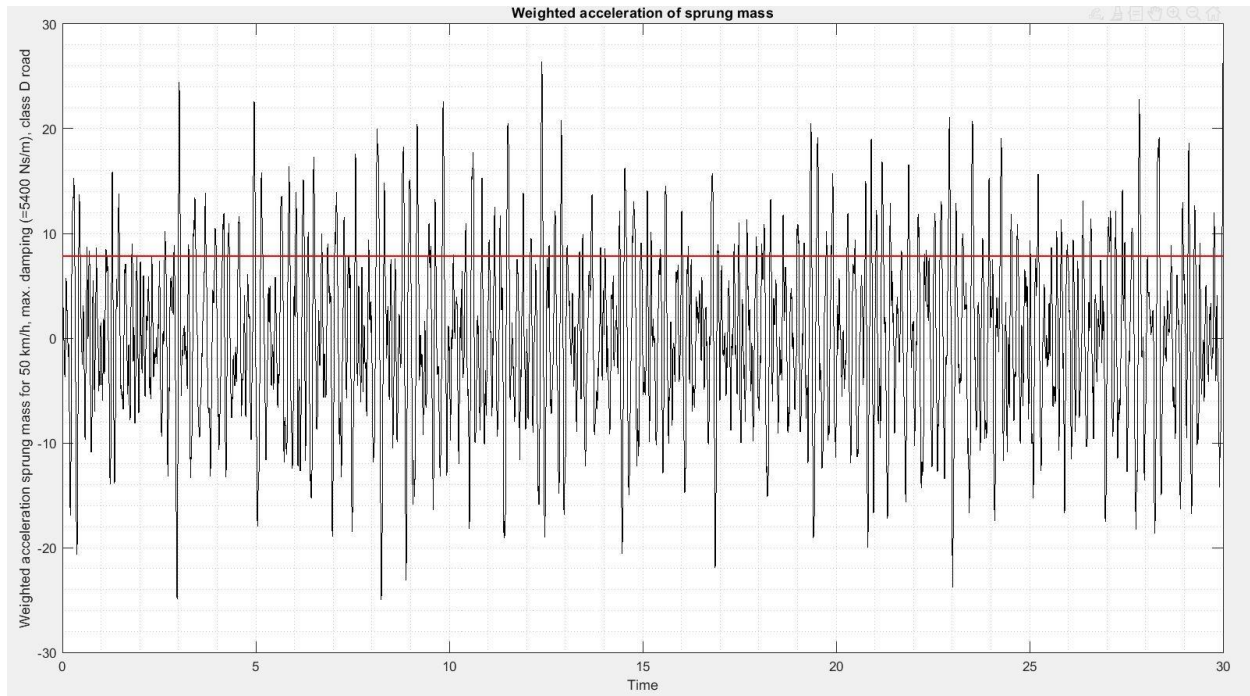


Fig. 3.5b Weighted sprung mass acceleration at road grade D

For the next simulation, the velocity was again kept at 50 km/h and the damping coefficient was taken as $c = 5400$ Ns/m. This time the road grade was changed from B (good) to D (poor). It can be observed from the Fig. 3.5a and Fig. 3.5b, that there is a significant increase in the weighted sprung mass acceleration value (rms) as we go from a good road surface (B) to more irregular road surface (D).

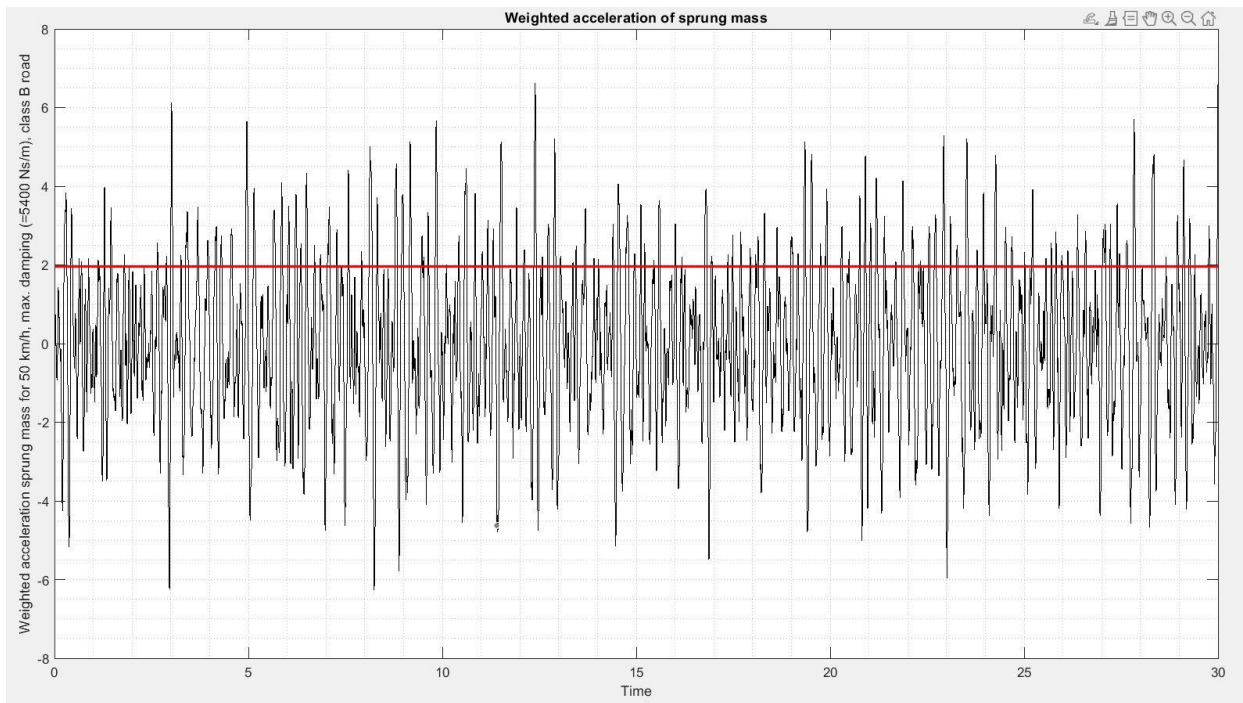


Fig. 3.6a Weighted sprung mass acceleration at 50 km/h

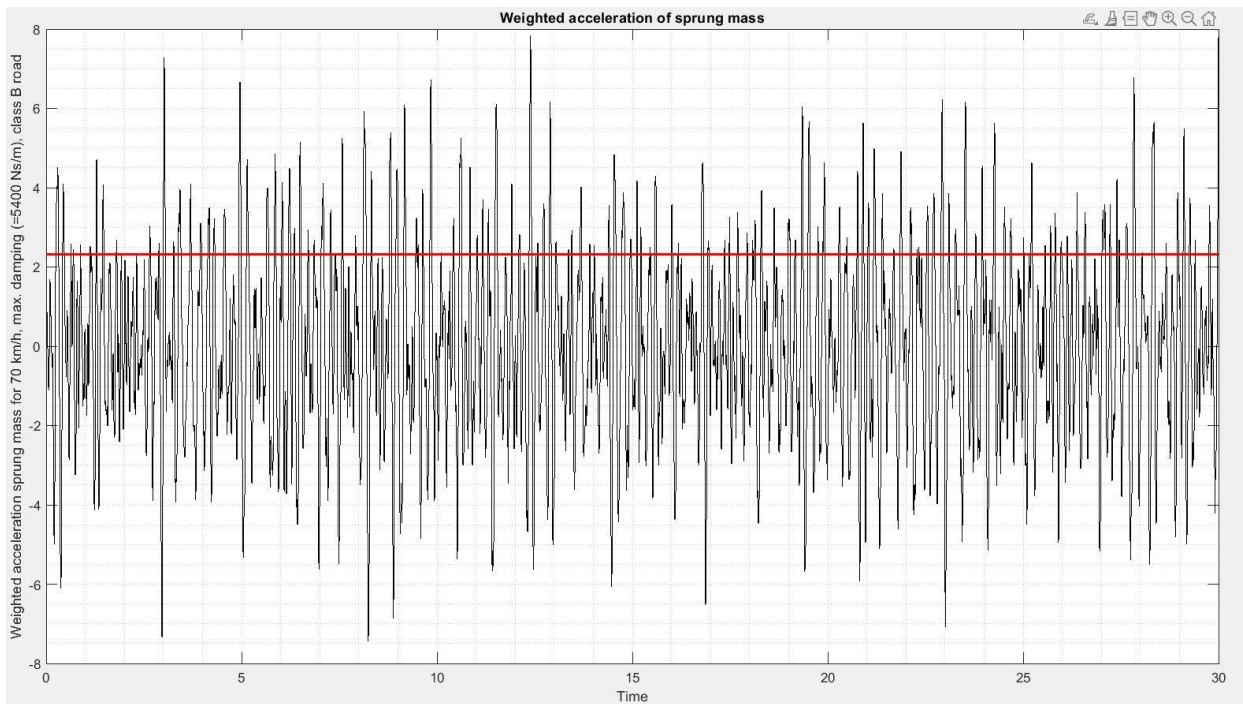


Fig. 3.6b Weighted sprung mass acceleration at 70 km/h

Finally, for the last simulation, the road grade was selected as B and the damping coefficient as $c = 5400$ Ns/m. This time the velocity was changed from 50 km/h to 70 km/h. As it is evident from the Fig. 3.6a and Fig. 3.6b, there is a slight increase in the weighted sprung mass acceleration rms value when the velocity is increased.

At the end, the simulation results for the Simulink and the Simscape models were compared to ensure the proper working of the model. The results are reported in the following tables.

Final results comparison:

	Simulink	Simscape
Power harvested	19.6455 W	19.6621 W
Road holding parameter (rms)	0.2167	0.2168
Weighted sprung mass acc. (rms)	1.9601 m/s ²	1.9618 m/s ²

Table 3.1a Results considering $c = 5400$ Ns/m, $V = 50$ km/h, road grade B

	Simulink	Simscape
Power harvested	19.1088 W	19.1101 W
Road holding parameter (rms)	0.1633	0.1634
Weighted sprung mass acc. (rms)	1.3434 m/s ²	1.3436 m/s ²

Table 3.1b Results considering $c = 2700$ Ns/m, $V = 50$ km/h, road grade B

	Simulink	Simscape
Power harvested	313.0890 W	313.3642 W
Road holding parameter (rms)	0.8650	0.8657
Weighted sprung mass acc. (rms)	7.8247 m/s ²	7.8318 m/s ²

Table 3.2a Results considering $c = 5400$ Ns/m, $V = 50$ km/h, road grade D

	Simulink	Simscape
Power harvested	304.5263 W	304.5672 W
Road holding parameter (rms)	0.6520	0.6521
Weighted sprung mass acc. (rms)	5.3638 m/s ²	5.3640 m/s ²

Table 3.2b Results considering $c = 2700$ Ns/m, $V = 50$ km/h, road grade D

	Simulink	Simscape
Power harvested	27.4695 W	27.4937 W
Road holding parameter (rms)	0.2562	0.2564
Weighted sprung mass acc. (rms)	2.3179 m/s ²	2.3207 m/s ²

Table 3.3a Results considering $c = 5400$ Ns/m, $V = 70$ km/h, road grade B

	Simulink	Simscape
Power harvested	26.7165 W	26.7187 W
Road holding parameter (rms)	0.1931	0.1932
Weighted sprung mass acc. (rms)	1.5887 m/s ²	1.5890 m/s ²

Table 3.3b Results considering $c = 2700$ Ns/m, $V = 70$ km/h, road grade B

It is evident from that the results from the Simulink model as well as the Simscape model are very much similar, this means that the model works well.

3.2 Quarter car with lookup table

The main parameters considered again are the road holding parameter for evaluating the handling performance, and the weighted sprung mass acceleration for the ride comfort.

Road holding parameter

The simulation was performed for the road holding parameter for different conditions. The results are demonstrated in the following figures.

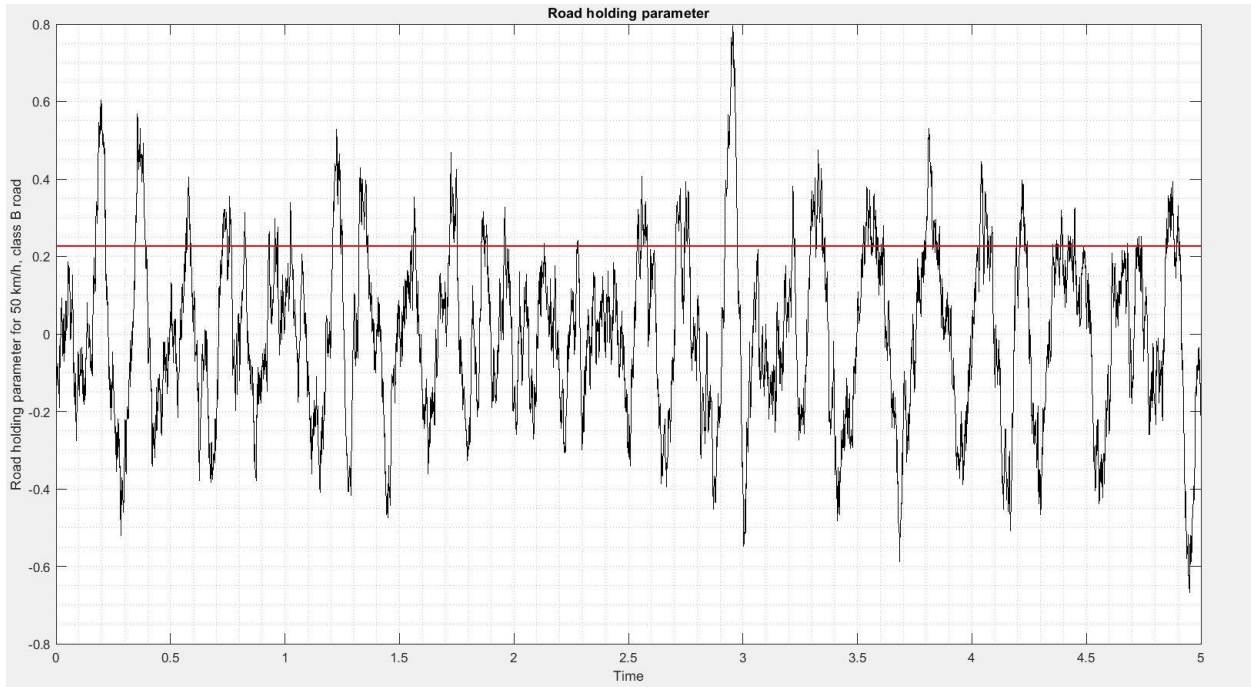


Fig. 3.7a Road holding parameter at 50 km/h and road grade B

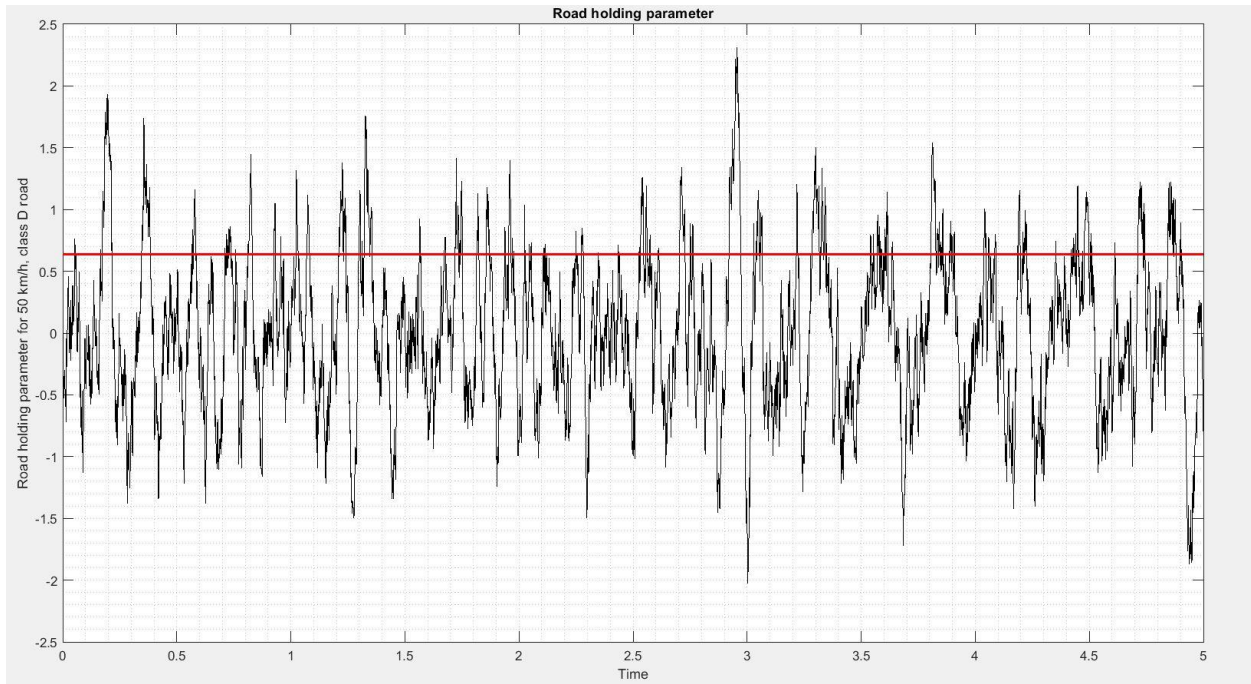


Fig. 3.7b Road holding parameter at 50 km/h and road grade D

The above simulations were carried out for a velocity of 50 km/h, only changing the road grade from B (good) to D (poor). From Fig. 3.7a and Fig. 3.7b, it can be noticed that there is a slight increment of the road holding parameter as we change from a good surface road (B) to a road surface with higher irregularities (D). In both the above plots, the road holding parameter remains well below 1, thus the wheel maintains good contact with the ground.

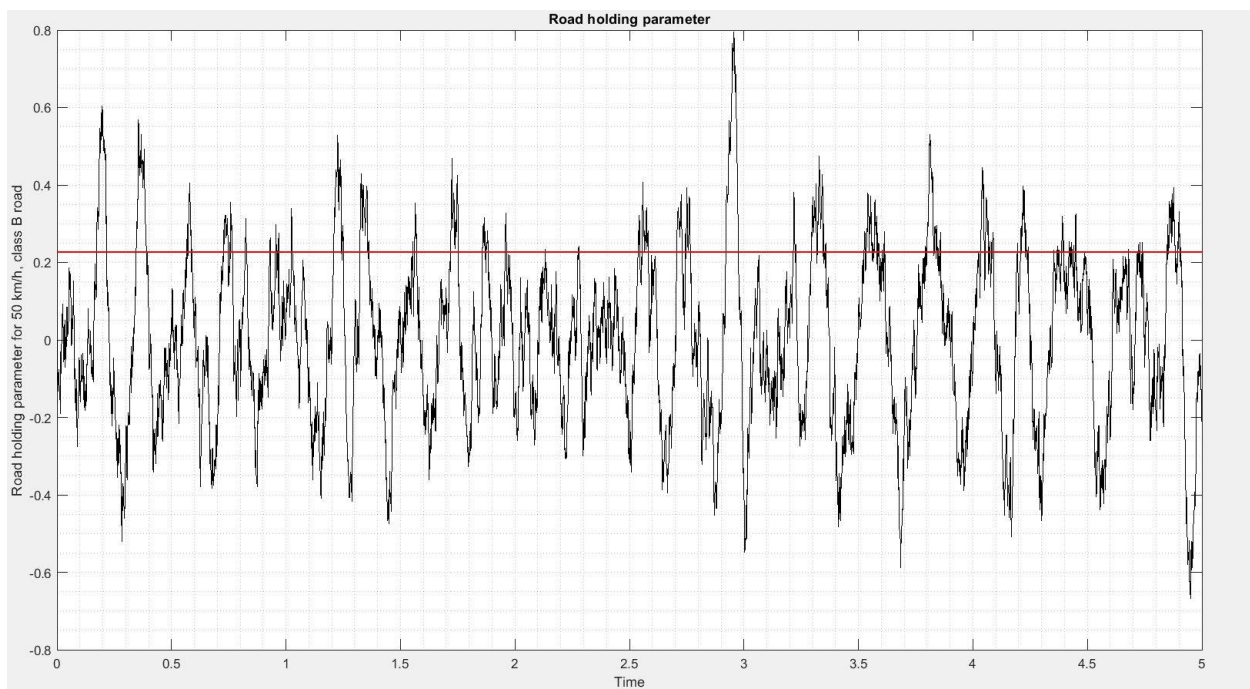


Fig. 3.8a Road holding parameter at 50 km/h and road grade B

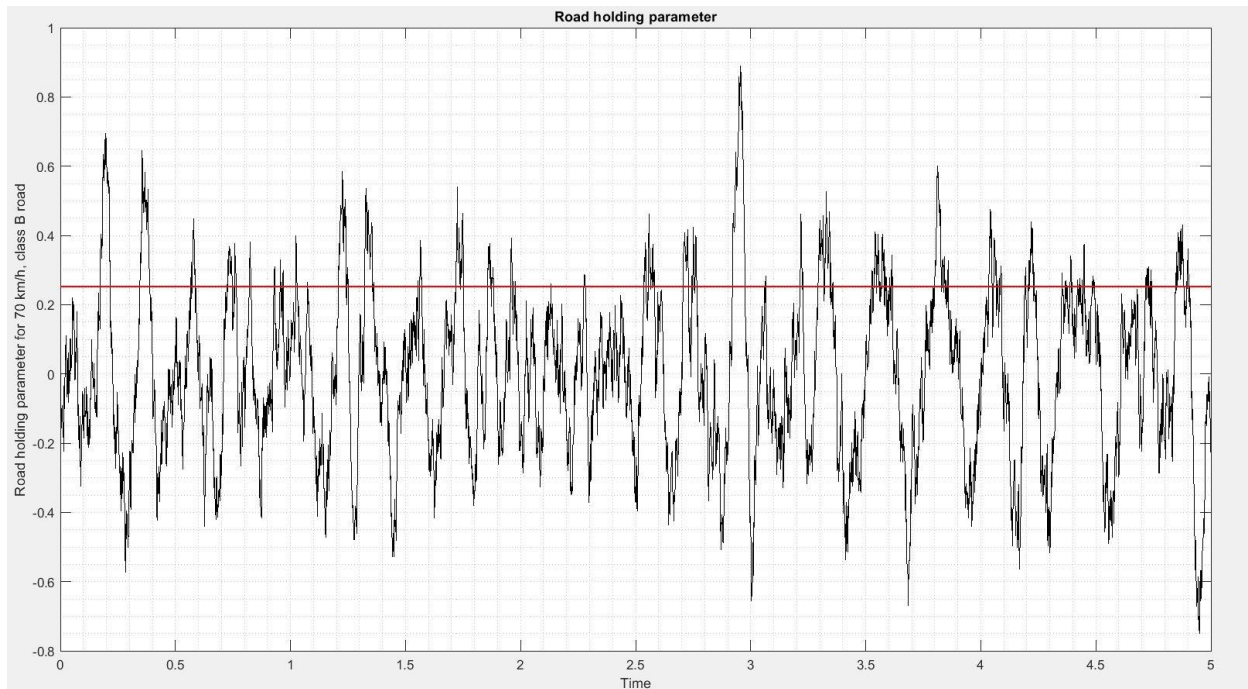


Fig. 3.8b Road holding parameter at 70 km/h and road grade B

Next, the simulations were performed for the same road grade B, but this time the velocity was changed from 50km/h to 70 km/h. It can be observed from Fig. 3.8a and Fig. 3.8b, that there is a slight increment in the road holding parameter as we increase the velocity. Here again, the road holding parameter is well below 1, which means the wheel remains in contact with ground.

Weighted acceleration of sprung mass

The ride comfort is evaluated as the RMS value of the acceleration of the vehicle body. The simulations performed for weighted sprung mass acceleration for different conditions are shown in the following figures.

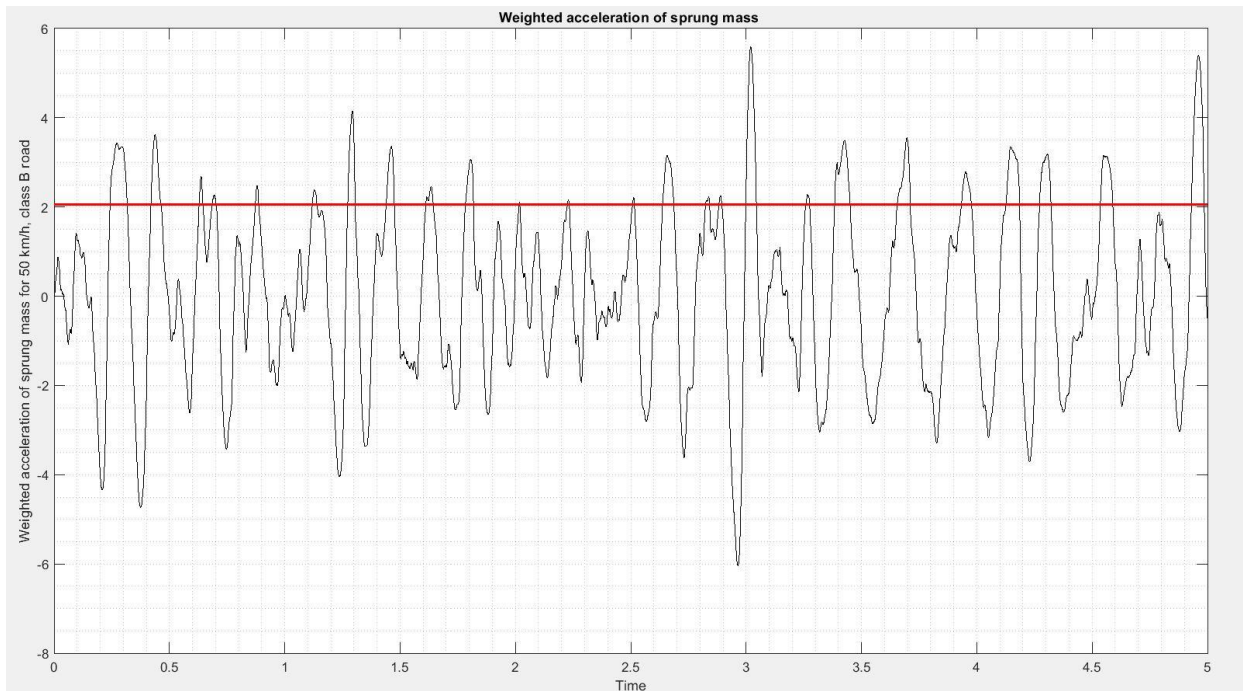


Fig. 3.9a Weighted sprung mass acceleration at 50 km/h and road grade B

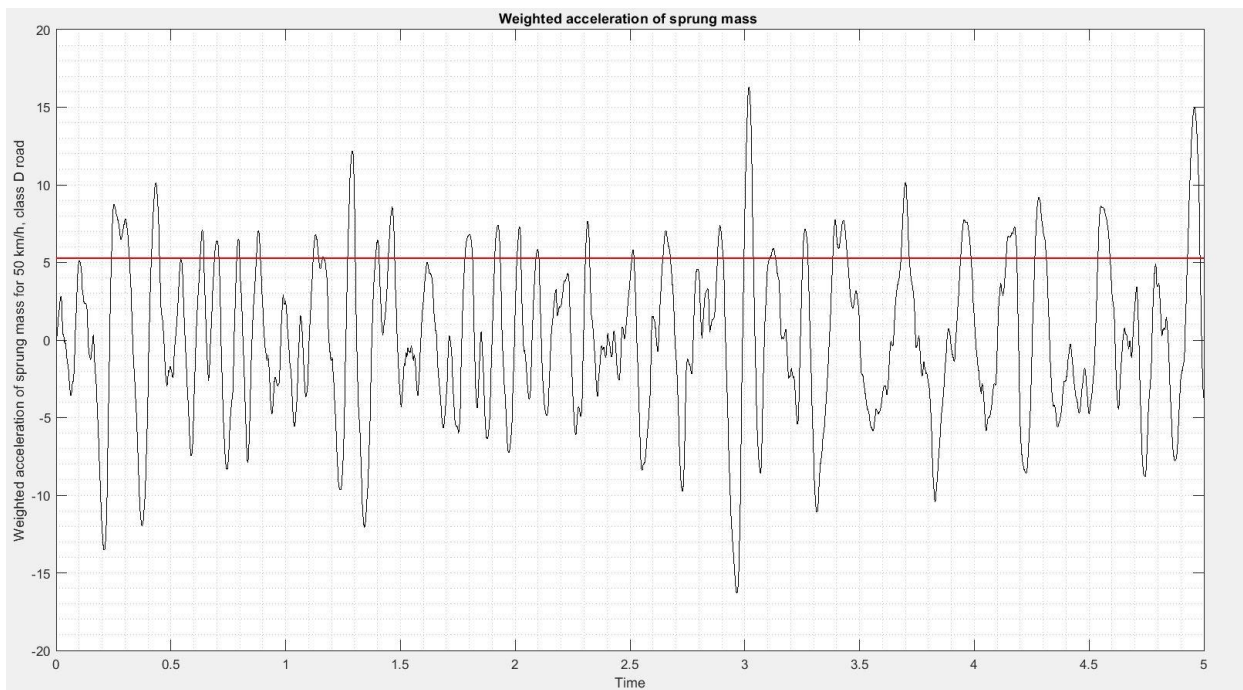


Fig. 3.9b Weighted sprung mass acceleration at 50 km/h and road grade D

First, the simulations were performed for the same velocity of 50 km/h, only the road grade was changed from B (good) to D (poor). In the Fig. 3.9a and Fig. 3.9b, it is evident that there is a significant increase of the weighted sprung mass acceleration when we change from a good road surface (B) to a poor road surface (D), as in the previous ideal quarter car model.

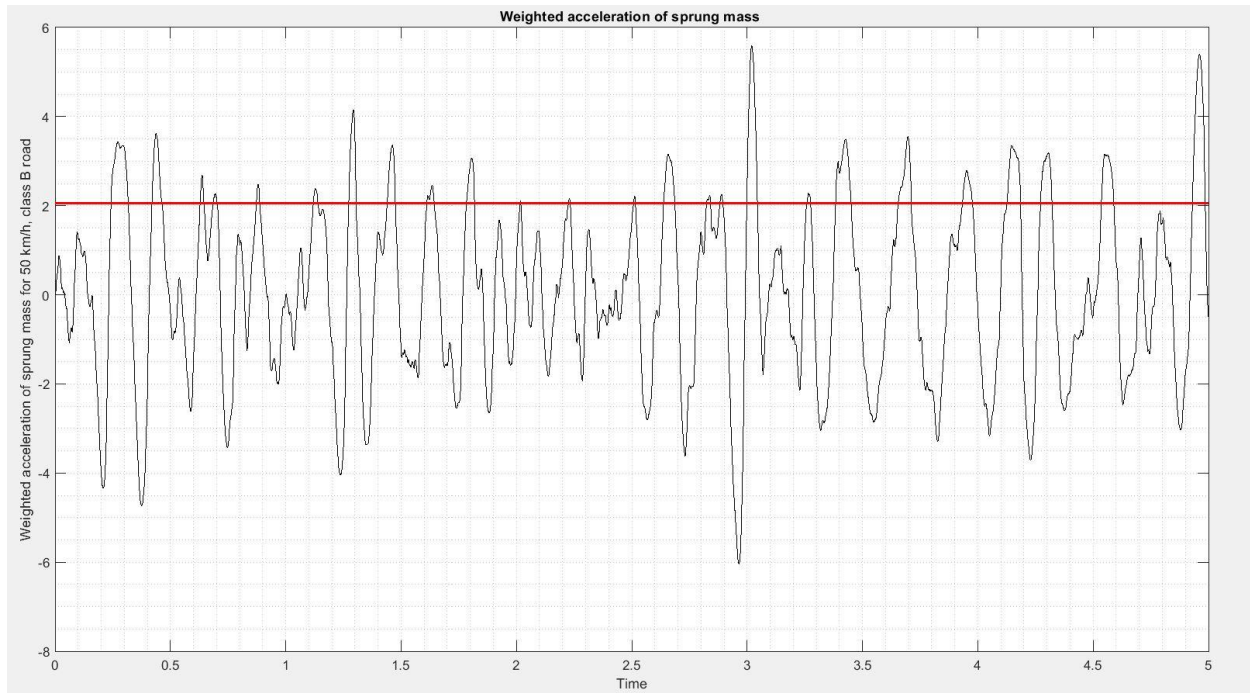


Fig. 3.10a Weighted sprung mass acceleration at 50 km/h and road grade B

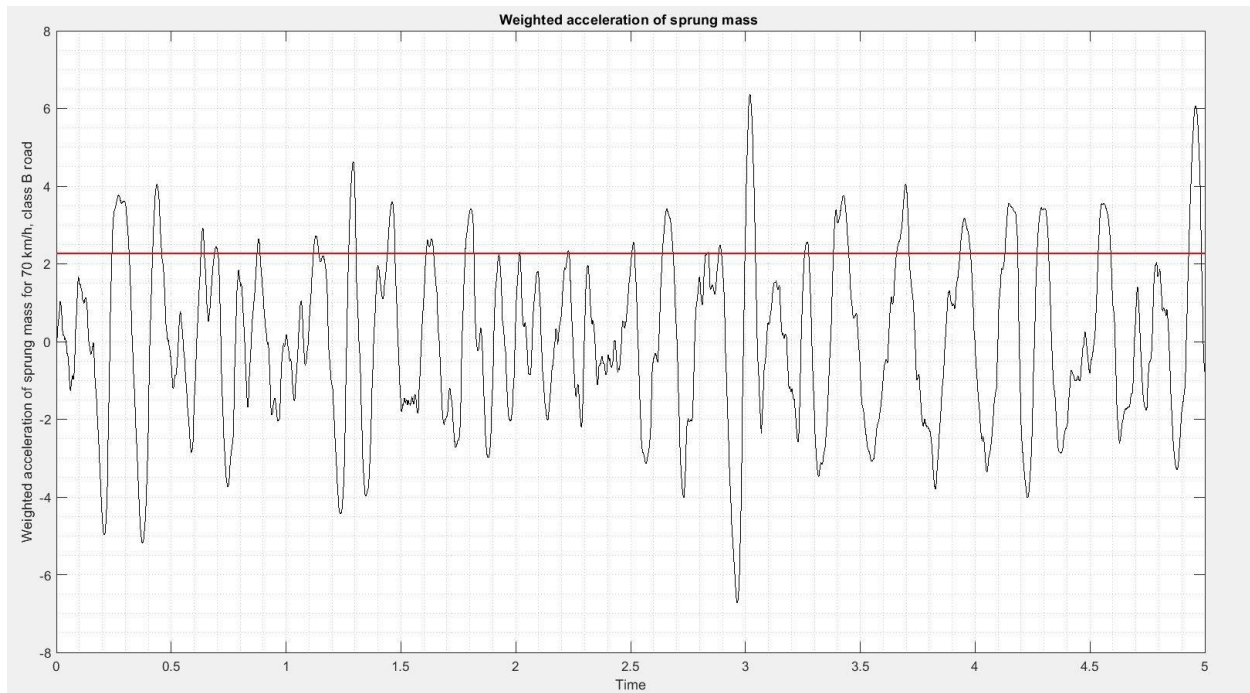


Fig. 3.10b Weighted sprung mass acceleration at 70 km/h and road grade B

For the next set of simulations, the road grade was selected as B, this time changing the velocity from 50 km/h to 70 km/h. A slight increment can be noticed from Fig. 3.10a and Fig. 3.10b, when we increase the velocity.

Finally, the simulations results of the Simulink model (with lookup table) and the Simscape model (with lookup table) were compared again to ensure the proper working of the model. The final results are reported in the following tables.

Final results comparison:

	Simulink	Simscape
V = 50 km/h, grade B		
Road holding parameter (rms)	0.2267	0.2299
Weighted sprung mass acc. (rms)	2.0569 m/s ²	2.0887 m/s ²
V = 70 km/h, grade B		
Road holding parameter (rms)	0.2522	0.2563
Weighted sprung mass acc. (rms)	2.2467 m/s ²	2.3051 m/s ²

Table 3.4 Results considering different velocities

	Simulink	Simscape
V = 50 km/h, grade B		
Road holding parameter (rms)	0.6307	0.6520
Weighted sprung mass acc. (rms)	5.2681 m/s ²	5.4058 m/s ²
V = 70 km/h, grade B		
Road holding parameter (rms)	0.7354	0.7508
Weighted sprung mass acc. (rms)	6.0036 m/s ²	6.1462 m/s ²

Table 3.5 Results considering different road grades

Once again, it can be observed from the results that the results of the Simulink and the Simscape models are very similar. Therefore, it can be concluded that the model is working well.

3.3 Quarter car with *skyhook*

For the *skyhook* control strategy, the actuator located between the two masses is responsible for providing both the damping coefficients c and c_s . The efficiency maps of the motor were also included, as already discussed in the previous section.

The objective of these simulations is to find the optimum combination of the damping coefficients c and c_s , so that we have a good trade-off between handling which is represented by the ‘road holding parameter’ and comfort which is represented by the ‘weighted sprung mass acceleration’.

To that end, firstly, a certain range of the damping coefficient c was fixed from 50 Ns/m to 1000 Ns/m, while the range of c_s was changed. The relevant plots are demonstrated below:

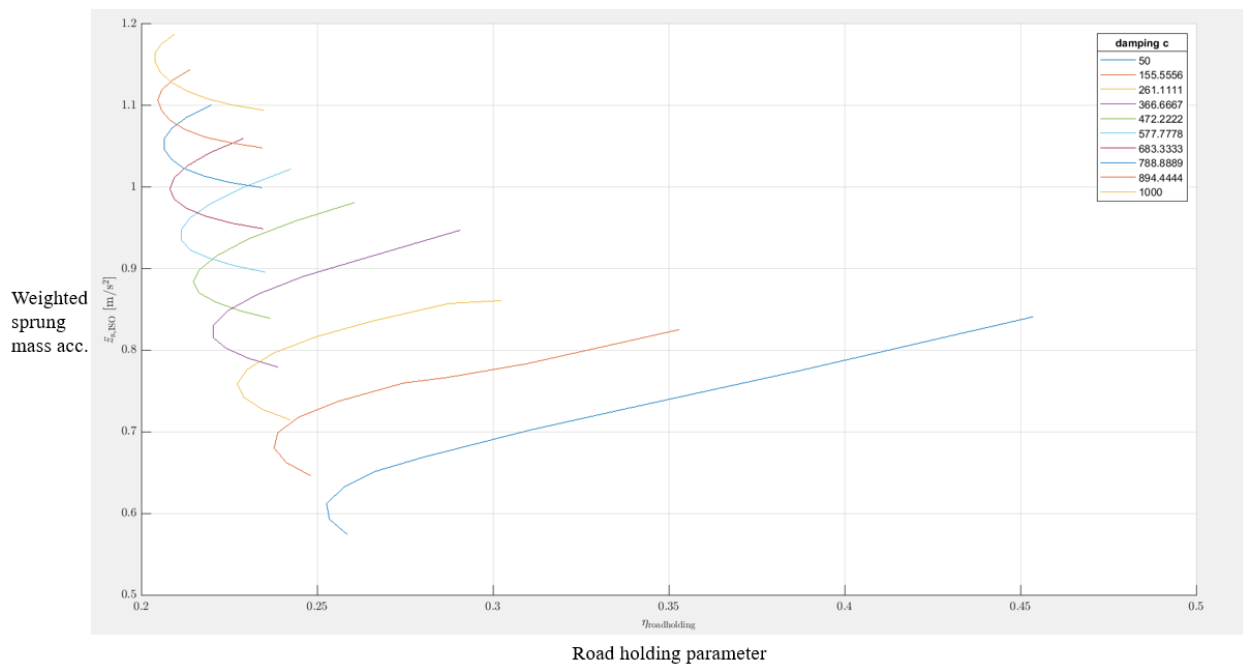


Fig. 3.11 Results considering c_s range between 8000-20000 Ns/m

The damping coefficient of the *skyhook* is plotted on the z-axis. The optimum results can be obtained along the envelope made by the knees of each curve in the Fig. 3.11.

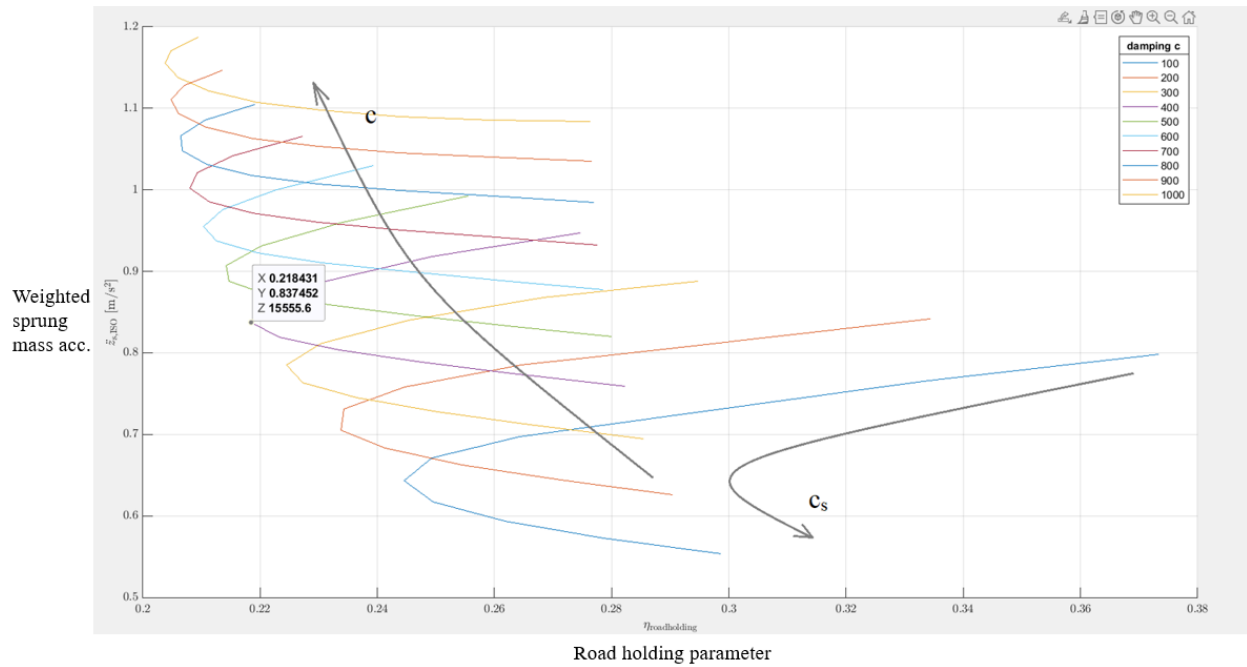


Fig. 3.12 Results considering c_s range between 8000-25000 Ns/m

In the Fig. 3.12, the arrows indicate the direction in which the damping coefficients c and c_s are increasing. The point highlighted in the plot is the best compromise between the handling and comfort performance for the considered ranges of c and c_s .

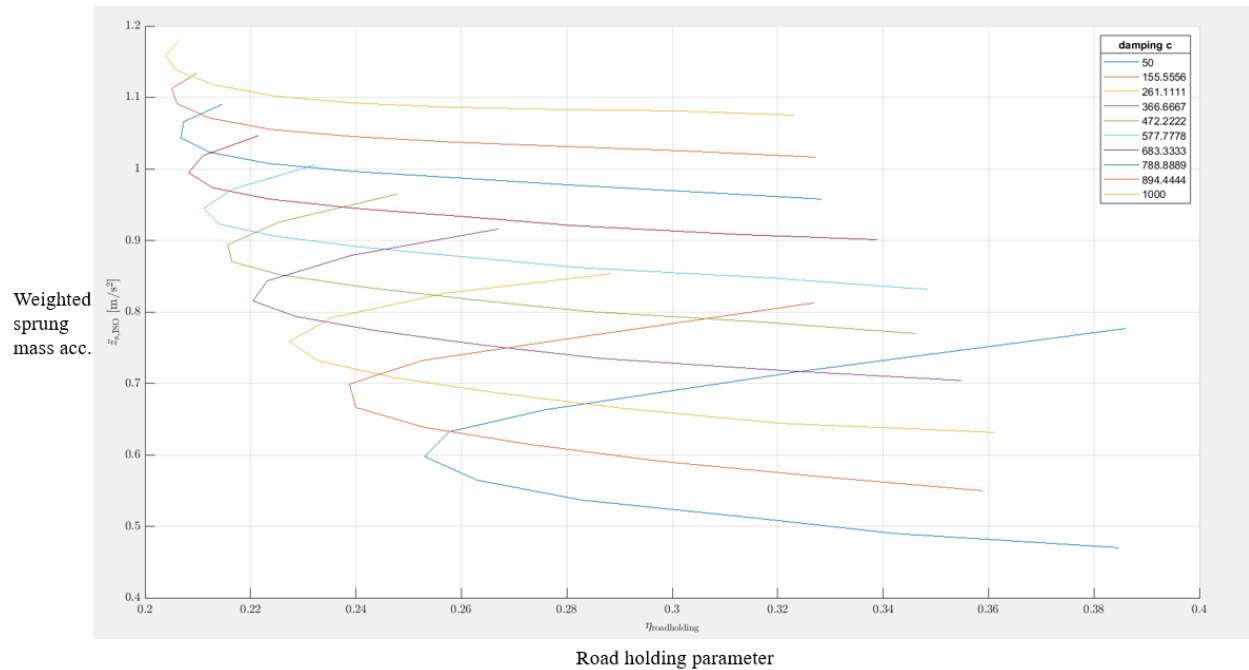


Fig. 3.13 Results considering c_s range between 9000-30000 Ns/m

As the c_s range increased, the rms values of the road holding parameter and the weighted acceleration also increased, which is not desirable. Because lower values of the road holding parameter translates to better adhesion of the wheel to the ground, so better handling; and lower values of the weighted sprung mass acceleration means better ride comfort.

For the next set of simulations, the range of the damping coefficient c_s was fixed to a certain range between 8000-25000 Ns/m, while the damping coefficient c was changed. Although, the results for what concerns the road holding parameter were good, but not so much promising for the weighted sprung mass acceleration, as the rms values came out to be slightly higher than the previous simulations.

3.4 Quarter car with *groundhook*

Similar to the *skyhook*, in the *groundhook* control strategy, the actuator located between the two masses is responsible for providing both the damping coefficients c and c_g .

The objective of these simulations is again to find the optimum combination of the damping coefficients c and c_g , so that we have a good trade-off between handling which is represented by the ‘road holding parameter’ and comfort which is represented by the ‘weighted sprung mass acceleration’.

The only difference this time is that the damping coefficient c is greater than c_g , while in the case of *skyhook* the damping coefficient c_s was greater than c . Otherwise, the results were coming out to be quite unstable with diverging behaviour in the plots.

Again, firstly, a certain range of the damping coefficient c was fixed from 1000 Ns/m to 2000 Ns/m, while the range of c_g was changed. The relevant plots are demonstrated below:

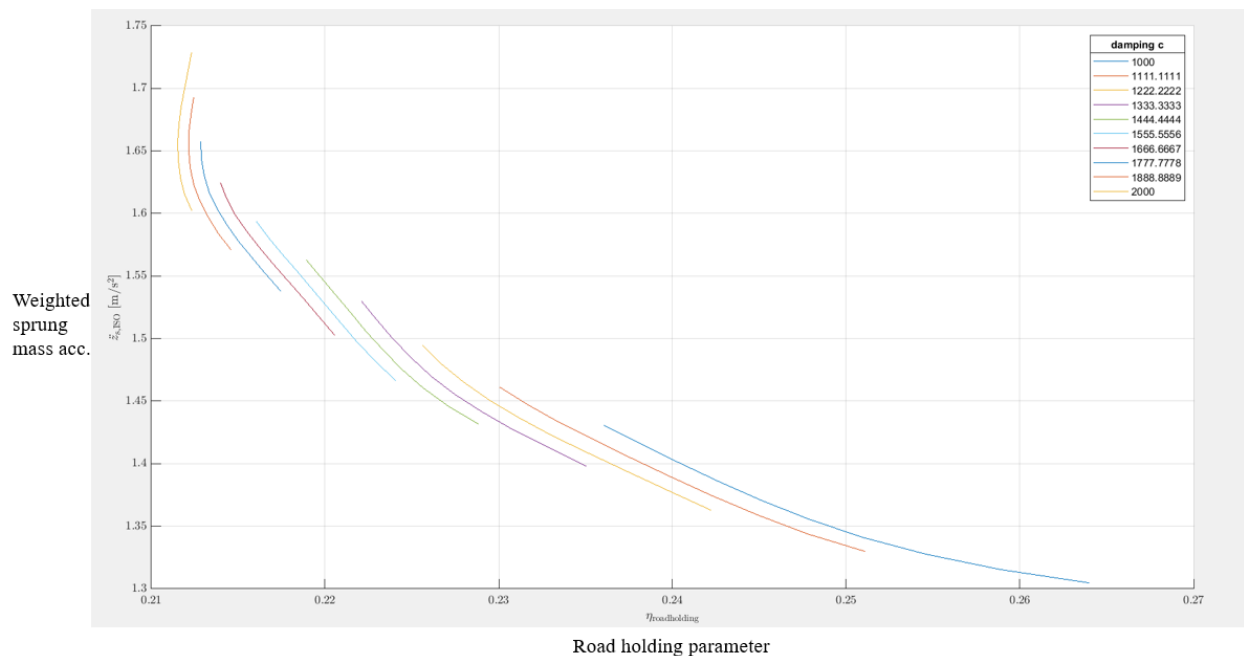


Fig. 3.14 Results considering c_s range between 100-500 Ns/m

The damping coefficient of the *groundhook* is plotted on the z-axis in the above plot. The optimum results can be obtained along the envelope made by the lower ends of each curve in the Fig. 3.14.

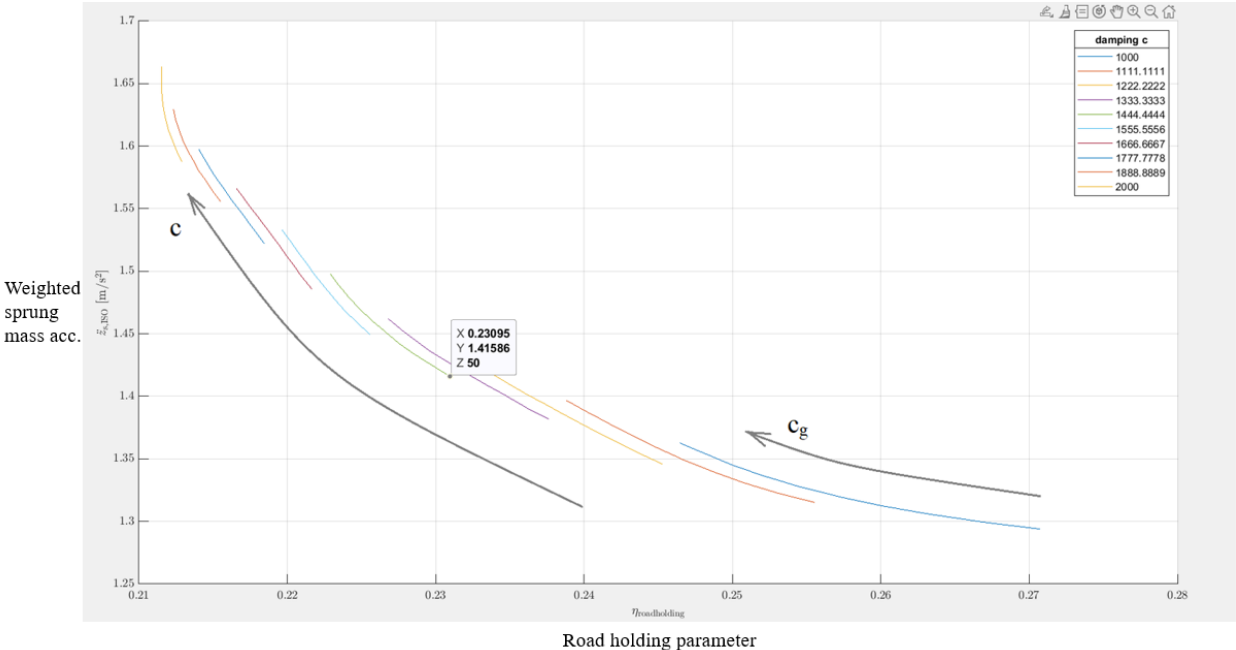


Fig. 3.15 Results considering c_s range between 50-300 Ns/m

The arrows in the Fig. 3.15 indicates the direction in which the damping coefficients c and c_g increases. The highlighted point in the plot gives the best trade-off between comfort and handling in the considered ranges of the damping coefficients c and c_g .

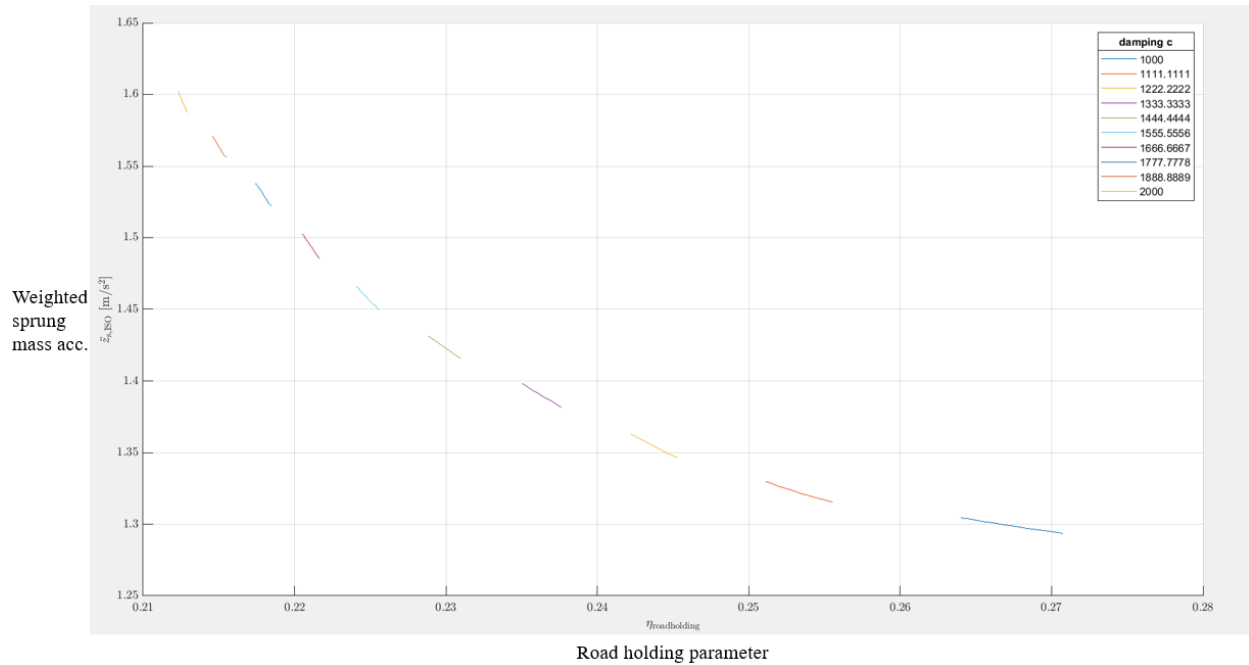


Fig. 3.16 Results considering c_s range between 50-100 Ns/m

As the range of the damping coefficient c_g decreased, the road holding parameter started to increase slightly. And the objective is to keep both the road holding parameter and the weighted sprung mass acceleration as low as possible, as already discussed. However, the rms values of the weighted sprung mass acceleration in case of *groundhook* control were higher in all simulations compared to the *skyhook* control.

Next set of simulations were performed keeping fixed the range of the damping coefficient c_g between 100-300 Ns/m, and changing the range of the damping coefficient c . The results of these simulations were acceptable for the road holding parameter, but not so good for the weighted sprung mass acceleration, as the rms values were even higher compared to the previous simulations.

Final results analysis:

For the analysis of the overall results of the quarter car model for the *passive* suspension (with lookup table), as well as the quarter car model for suspensions with *skyhook* and *groundhook* control strategies, all the significant results were extracted from the simulations and are reported in the Table 3.6. The rms values weighted sprung mass acceleration and road holding parameter were considered for the comparison of performance in terms of comfort and handling, respectively. While, for the actual power, the mean or average value was considered to compare the power harvesting capability.

	Passive	Skyhook – best comfort	Skyhook – best handling	Skyhook – best overall	Groundhook – best comfort	Groundhook – best handling	Groundhook – best overall
Weighted sprung mass acc. (rms) [m/s ²]	2.2546	1.0751	1.0944	1.0836	1.6024	1.7288	1.6639
Road hold parameter (rms)	0.253	0.3233	0.2349	0.2764	0.2123	0.2123	0.2115
Actual power (avg.) [W]	-16.17	-11.83	-13.31	-12.55	-19.64	-20.43	-19.96

Table 3.6 Final comparison of the simulation results

The negative sign for the Power indicates power dissipated in terms of *passive* damper, and power regenerated or power available to be harvested in case of the dampers with *skyhook* and *groundhook* control.

In the Table 3.6, the highlighted column “Skyhook – best overall” indicates the best trade-off between best comfort and best handling results for the *skyhook* control strategy. Similarly, the highlighted column “Groundhook – best overall” reports the best compromise between the best comfort and best handling results for the *groundhook* control strategy.

The overall performance of both the active control strategies are better compared to the passive suspension. Therefore, the results of the active control strategies are discussed further. Considering the weighted sprung mass acceleration, the performance of the *skyhook* is better than the *groundhook* control, because the lower is the weighted sprung mass acceleration, the more comfortable is the ride.

For the road holding capability, the performance of the *groundhook* is slightly better compared to the *skyhook* control, because the lower is the value of the road holding parameter, the better is the contact between the tire and the road surface.

In case of the power regenerated or power harvested, the *groundhook* outperforms the *skyhook* control. Since both control strategies are active control, they work in all four quadrants of the Force-velocity curve (Fig. 1.14 in Section 1). The *skyhook* control works more in the quadrants for active region of the Force-velocity curve, and thus it has lower regenerated power compared to the *groundhook* control, because the *groundhook* control works more in the quadrants for passive region of the Force-velocity curve, where the regenerated power is obtained from the otherwise dissipated power.

4. Conclusions

Starting with the introduction, different types of front and rear motorcycle suspension systems are described. After that, types of controlled suspensions including active, semi-active and regenerative suspension systems were discussed. Then this thesis work focuses on the modelling procedure of an electromagnetic regenerative damper for motorcycle suspensions.

The objective of this work has been to study the behaviour of the damper in dynamic conditions, and to assess the performance by implementing some control strategies.

To that end, Section 2 deals with the development of quarter car model for ideal and real passive suspension systems is described, along with the Simscape models to compare and further validate the theoretical models developed in Simulink. Then the quarter car modelling for the active *skyhook* and active *groundhook* control strategies for real-world applications is discussed.

In the Section 3, the simulation results of the ideal quarter car model and quarter car model with lookup table were compared with the respective Simscape models, with the help of corresponding plots and tables along with some descriptions. Finally, the simulation results and the relevant plots for the quarter car models with active *skyhook* and active *groundhook* control strategies were discussed.

For a comprehensive comparison for the assessment of overall performance of the quarter car model for the *passive* suspension (with lookup table), as well as the quarter car model for suspensions with *skyhook* and *groundhook* control strategies, all the significant results were extracted from the simulations and are reported in a table (Table 3.6). The results came out to be satisfactory.

Final conclusions that can be derived on the basis of the Table 3.6 are:

- For weighted acceleration of sprung mass, the dampers with *skyhook* and *groundhook* control are clearly better than the passive damper. But especially the *skyhook* control provides the best results with lower accelerations. This outcome was as expected, because the *skyhook* control is known for better comfort since they provide better damping of the sprung mass.
- In case of the road holding parameter, the results are comparable with not very significant differences. However, the *groundhook* control provides slightly better performance. Therefore, it can be said that *groundhook* control is slightly better than the *skyhook* in terms of road holding capability or handling performance, which is more important in case of motorcycles.
- For what concerns the power regenerated, again the *groundhook* control provides slightly better results in terms of power regenerating capability as compared to the *skyhook* one.

List of Figures

1.1 All head stock mounted forks have these types of deflection to some degree, due to the large lever arm [2]	2
1.2 Examples of front suspensions [1]	3
1.3 Examples of USD forks [2]	4
1.4 In leading link forks, the relative heights of link pivots and wheel spindle decides the wheel travel path [2]	5
1.5 Examples of leading link forks [2]	6
1.6 Examples of trailing link forks [2]	7
1.7 Difazio hub-centre steering on a 500 cc Suzuki-powered racer is shown [2]...	8
1.8 Different types of construction used in double link [2]	9
1.8a Hossack/Fior/Foale/Britten suspension [2]	9
1.9 McPherson strut-based suspension [2]	10
1.9a BMW Telelever [2]	11
1.10 The left sketch represents the system based on virtual steering axis and the right one represents a normal head stock steering design. The ellipses represent tyre contact patches. The grey lines depict the steering in the straight ahead position and the black ones depict it steered to 20 degrees approximately. Both drawings show the projection on the ground. [2]	12
1.11 Examples of rear suspensions [1]	13
1.12 One of the interpretations of the ‘cantilever monoshock’, by Yamaha [2] ..	14
1.13a BMW’s early version of the single sided swing arm for shaft drive [2] ...	16
1.13b BMW’s “paralever”, the later model [2]	16

1.14 Force–velocity regions for active, semi-active and passive damping. Here, the velocity is the relative speed between the car body and the wheel [8]	20
1.15a Model scheme of the electrohydrostatic regenerative shock absorber	21
1.15b Section view from the prototype of a gerotor pump unit of the electrohydrostatic regenerative shock absorber	22
2.1 Quarter Car Model with two degrees of freedom	24
2.2 Simulink block scheme of the model	27
2.3 Simscape model scheme	30
2.4 Force-velocity characteristic (lookup table)	31
2.5 Quarter car model with a controlled damper	32
2.6 Passive damper with the lookup table	32
2.7 Simscape model with lookup table	33
2.8 a) Ideal <i>skyhook</i> without the conventional shock absorber, b) with the conventional shock absorber [3]	35
2.9 <i>Skyhook</i> with semi-active damper for real-world application [3]	36
2.10 Active <i>skyhook</i> model with a controlled actuator supplying all the force exerted between the sprung and unsprung masses	37
2.11 Block scheme of the model with motor efficiency map and actuator force ..40	
2.12 Ideal <i>groundhook</i> with a damper located between the unsprung mass and the contact point with the ground [3]	42
3.1 Road holding parameter comparison for different damping coefficients	44
3.2 Road holding parameter comparison for different road grade	45
3.3 Road holding parameter comparison for different velocity	46
3.4a Weighted sprung mass acceleration at $c = 5400 \text{ Ns/m}$	47

3.4b	Weighted sprung mass acceleration at $c = 2700$ Ns/m	47
3.5a	Weighted sprung mass acceleration at road grade B	48
3.5b	Weighted sprung mass acceleration at road grade D	49
3.6a	Weighted sprung mass acceleration at 50 km/h	50
3.6b	Weighted sprung mass acceleration at 70 km/h	50
3.7a	Road holding parameter at 50 km/h and road grade B	54
3.7b	Road holding parameter at 50 km/h and road grade D	54
3.8a	Road holding parameter at 50 km/h and road grade B	55
3.8b	Road holding parameter at 70 km/h and road grade B	56
3.9a	Weighted sprung mass acceleration at 50 km/h and road grade B	57
3.9b	Weighted sprung mass acceleration at 50 km/h and road grade D	57
3.10a	Weighted sprung mass acceleration at 50 km/h and road grade B	58
3.10b	Weighted sprung mass acceleration at 70 km/h and road grade B	59
3.11	Results considering c_s range between 8000-20000 Ns/m	61
3.12	Results considering c_s range between 8000-25000 Ns/m	62
3.13	Results considering c_s range between 9000-30000 Ns/m	63
3.14	Results considering c_s range between 100-500 Ns/m	64
3.15	Results considering c_s range between 50-300 Ns/m	65
3.16	Results considering c_s range between 50-100 Ns/m	66

List of Tables

2.1 Quarter car model parameters for front suspension of a motorcycle	25
2.2 Road roughness coefficient	29
2.3 Velocities	29
3.1a Results considering $c = 5400$ Ns/m, $V = 50$ km/h, road grade B	51
3.1b Results considering $c = 2700$ Ns/m, $V = 50$ km/h, road grade B	51
3.2a Results considering $c = 5400$ Ns/m, $V = 50$ km/h, road grade D	52
3.2b Results considering $c = 2700$ Ns/m, $V = 50$ km/h, road grade D	52
3.3a Results considering $c = 5400$ Ns/m, $V = 70$ km/h, road grade B	52
3.3b Results considering $c = 2700$ Ns/m, $V = 70$ km/h, road grade B	53
3.4 Results considering different velocities	60
3.5 Results considering different road grades	60
3.6 Final comparison of the simulation results	67

Bibliography

[1] Mara Tanelli, Matteo Corno, and Sergio Saveresi, “Modelling, Simulation and Control of Two-Wheeled Vehicles”, 2014.

[2] Tony Foale, “Motorcycle Handling and Chassis Design”, 2002.

[3] Giancarlo Genta, Lorenzo Morello, “The Automotive Chassis Volume 2: System Design”, 2009.

[4] Galluzzi, R., Tonoli, A., Amati, N., Curcuruto, G. et al., "Regenerative Shock Absorbers and the Role of the Motion Rectifier", 2016.

[5] Lei Zuo, Pei-Sheng Zhang, “Energy Harvesting, Ride Comfort, and Road Holding of Regenerative Vehicle Suspensions”, 2013.

[6] Manfredi Tornabene, Thesis project “Rotary Regenerative Shock Absorber for Automotive Applications: Control Strategies and Hardware-In-the-Loop Implementation”, 2021

[7] Giancarlo Genta, Lorenzo Morello, “The Automotive Chassis Volume 1: Components Design”, 2009.

[8] Mats Jonasson, Fredrik Roos, “Design and evaluation of an active electromechanical wheel suspension system”, 2007.